

A globally convergent Carleman–Picard method for an inverse initial-value problem for a nonlinear diffusive coagulation–fragmentation equation

Thuy T. Le* Minh-Binh Tran† Loc H. Nguyen‡

Abstract

We study an inverse initial-density problem for a nonlinear diffusive coagulation–fragmentation equation with known coagulation and fragmentation kernels. The objective is to recover the unknown initial particle-size distribution on a finite interval from time-dependent boundary observations of the solution and its size derivative. To solve this inverse problem, we develop a globally convergent numerical method based on a Legendre–exponential time reduction and a Carleman–Picard iteration. The time reduction transforms the original problem into a nonlinear coupled system for the spatial mode coefficients, while the Carleman weight and the corresponding Carleman estimate guarantee the global convergence of the Picard iteration without requiring a good initial guess. We prove the convergence of the proposed method and obtain a complete reconstruction procedure for the initial density. Numerical experiments with noisy boundary data demonstrate that the method yields accurate and stable reconstructions for several representative test profiles.

1 Introduction

Let $T > 0$ be a final time, and let

$$f : (0, \infty) \times (0, T) \rightarrow \mathbb{R}$$

denote the density of particles of size v at time t . In coagulation–fragmentation models, the density f evolves under the combined effects of coagulation, fragmentation, convection in the size variable, and diffusion in the size variable. In our work, those effects are incorporated into the following coagulation–fragmentation equation with size convection–diffusion [28, 34, 42]:

$$\begin{cases} \partial_t f(v, t) = -b(v)\partial_v f(v, t) + \partial_{vv} f(v, t) + Q(f)(v, t), & (v, t) \in (0, \infty) \times (0, T), \\ f(0, t) = 0, & t \in (0, T), \\ f(v, 0) = f^0(v), & v \in (0, \infty), \end{cases} \quad (1.1)$$

where f^0 denotes the initial particle-size distribution. The operator $Q(f)$ is decomposed as

$$Q(f)(v, t) = Q_{\text{coag}}(f)(v, t) + Q_{\text{frag}}(f)(v, t), \quad (1.2)$$

where

$$Q_{\text{coag}}(f)(v, t) = \frac{1}{2} \int_0^v K(v - v^*, v^*) f(v - v^*, t) f(v^*, t) dv^* - f(v, t) \int_0^\infty K(v, v^*) f(v^*, t) dv^*, \quad (1.3)$$

and

$$Q_{\text{frag}}(f)(v, t) = -f(v, t) \int_0^v V(v - v^*, v) dv^* + 2 \int_0^\infty V(v, v^*) f(v + v^*, t) dv^*. \quad (1.4)$$

*Department of Mathematics and Statistics, California State University, Long Beach, CA 90032, USA, Thuy.Le@csulb.edu.

†Department of Mathematics, Texas A&M University, College Station, TX 77843, USA, minhbinh@tamu.edu

‡Department of Mathematics and Statistics, University of North Carolina at Charlotte, NC 28223, USA, loc.nguyen@charlotte.edu

The microscopic structure of the system is encoded in the nonnegative kernels

$$K(v, v^*) \geq 0, \quad V(v, v^*) \geq 0,$$

which are assumed to be symmetric in v and v^* . The kernel K describes the coagulation rate at which two clusters of sizes v and v^* merge to form a single cluster of size $v + v^*$, whereas V characterizes the fragmentation rate at which a cluster of size $v + v^*$ breaks into two clusters of sizes v and v^* . Interactions with the surrounding medium, allowing for the exchange of monomeric units, are modeled by the size-convective term $-b(v)\partial_v f(v, t)$ and the size-diffusive term $\partial_{vv} f(v, t)$.

Equation (1.1) and related coagulation–fragmentation models have been extensively investigated in both theoretical and numerical settings; see, for instance, [5, 6, 7, 11, 13, 19, 25, 36, 35, 43, 45, 46, 50, 53] and the references therein. For broader surveys and additional references, we refer the reader to [7, 8, 12].

In this paper, we propose a globally convergent method for an inverse initial-value problem associated with (1.1). Let $L > 0$ be fixed, and assume that the unknown initial density f^0 is supported in $[0, L]$, that is, $f^0(v) = 0$ for all $v > L$. We assume that the coagulation and fragmentation kernels are known. Using time-dependent boundary observations of the solution and its size derivative at $v = 0$ and $v = L$, we aim to reconstruct f^0 on $[0, L]$.

Problem 1 (Inverse initial-density problem). *Let f be a sufficiently smooth solution of (1.1)–(1.4). Given the time-dependent boundary observations*

$$\phi_0(t) := f(0, t), \quad \phi_L(t) := f(L, t), \quad \psi_0(t) := \partial_v f(0, t), \quad \psi_L(t) := \partial_v f(L, t), \quad (1.5)$$

for $t \in (0, T)$, determine the unknown initial density f^0 on $[0, L]$.

This inverse problem is of practical interest because direct measurement of the full particle density $f(v, t)$ over the entire size–time domain is generally expensive and difficult to implement. In many realistic situations, it is far more feasible to collect data only at a few accessible observation points, such as the boundary locations $v = 0$ and $v = L$. If the initial density f^0 can be successfully reconstructed from such limited measurements, then it can be extended by zero for $v > L$, and the full evolution of the particle system can subsequently be computed by solving the forward problem (1.1) with existing analytical [8] or numerical methods [16, 20]. In this way, one can recover the particle density across the entire domain while significantly reducing experimental cost and measurement effort.

Problem 1 is extremely challenging. One source of difficulty is the nonlinear collision operator $Q(f)$, whose complicated integro-differential structure makes the forward map from the initial density to the boundary observations highly nonlinear. In principle, one may apply a conventional least-squares approach together with Tikhonov regularization. However, the resulting cost functional is generally nonconvex and may possess multiple local minima. Therefore, such an approach is only locally convergent and typically requires a good initial guess, which is often unavailable in practice. In addition, inverse problems with boundary measurements are usually ill-posed, meaning that small noise in the data can lead to large reconstruction errors. This severe instability poses an additional obstacle to the reliable recovery of f^0 . To overcome these difficulties, we develop a globally convergent reconstruction framework for Problem 1 based on two main ingredients: a Legendre–exponential time reduction and a Carleman–Picard iterative procedure. The global convergence of the method is guaranteed by the use of a Carleman weight, together with suitable Carleman estimates, which provide the key mechanism for controlling the reconstruction process without requiring a good initial guess. On the other hand, the ill-posedness of the inverse problem is mitigated by truncating the Fourier expansion of the data with respect to the polynomial–exponential basis, thereby filtering out highly oscillatory noise components. As a result, the original inverse problem is reduced to a finite, coupled system of equations for the mode coefficients, which can then be solved stably and effectively.

The idea of combining time reduction with Carleman estimates was first introduced in [32], where an inverse initial-value problem for a quasilinear parabolic equation was solved. Later, in [38], it was observed that the approach developed in [32] can in fact be interpreted as the construction of a contraction mapping whose fixed point is the desired solution. As a consequence, the associated Picard iteration converges globally, even when the initial guess is far from the true solution. Since then, this framework has been extended to a variety of inverse problems; see, for example, [1, 30, 33, 40, 48, 49]. The Carleman–Picard method was further generalized to nonlinear inverse problems for hyperbolic equations in [31, 39]. In particular, the

approach developed in [31] was shown to apply to experimental data. However, these earlier methods are not directly applicable to Problem 1 because of the strong nonlinearity and complicated integro-differential structure arising from the coagulation and fragmentation effects. The main contribution of the present paper is to develop a Carleman–Picard method tailored to this coagulation–fragmentation model.

We now briefly review the literature most relevant to the present work. Since the 1970s, inverse problems for coagulation–fragmentation models have attracted considerable attention in the broader scientific community [37, 44]. Most existing mathematical studies are concerned with inverse problems for linear (fragmentation-only) or linearized versions of the model; see, e.g., [2, 4, 5, 9, 10, 14, 17, 18, 24, 27, 41]. Moreover, the data used in these works are typically internal measurements rather than boundary observations of the type considered in Problem 1. Inverse results for nonlinear coagulation–fragmentation models are much more limited, and the existing approaches also appear to rely on internal data (see, for instance [3, 22, 26, 51, 52]). To the best of our knowledge, we have not found any work on inverse problems for full coagulation–fragmentation equations that uses only boundary measurements as in our setting.

The remainder of the paper is organized as follows. In Section 2, we present the main analytical ingredients used throughout the paper, including a one-dimensional Carleman estimate, the Legendre–exponential basis for time-dimensional reduction, and Lipschitz estimates for the projected coagulation and fragmentation operators. In Section 3, we eliminate the time variable and derive a reduced coupled system of ordinary differential equations for the expansion coefficients. In Section 4, we introduce the Carleman–Picard iteration for solving the reduced inverse problem and prove its global convergence. In Section 5, we describe the numerical implementation of the method, explain the generation of synthetic boundary data, and present several numerical experiments to validate the proposed reconstruction procedure. Finally, Section 6 contains the concluding remarks.

2 Carleman estimate, Legendre–exponential basis, and Lipschitz estimates

In this section, we present several analytical ingredients needed to design a numerical solver for Problem 1. We first present a one-dimensional Carleman estimate. We then present the Legendre–exponential basis used for the time-dimensional reduction and introduce the projected system. Finally, we establish Lipschitz estimates for the projected coagulation and fragmentation operators on the admissible set. The Carleman estimate and these Lipschitz bounds play a crucial role in proving the global convergence of the Carleman–Picard method developed in Section 4.

2.1 A one-dimensional Carleman estimate

We summarize a one-dimensional Carleman estimate, which will be the main analytical tool in the Carleman–Picard method developed later. Fix $L > 0$ and choose $v_0 < 0$. Define $r(v) := v - v_0, v \in [0, L]$, so that $r(v) > 0$ on $[0, L]$. For parameters $\lambda > 0$ and $\beta > 0$, we introduce the Carleman weight $e^{2\lambda r(v)^{-\beta}}$, which is used to weight the energy terms in the Carleman estimate stated below. The estimate below provides weighted control of u and its derivatives in terms of u'' (up to boundary terms), and will be used to ensure stability and convergence of our reconstruction scheme.

Lemma 1 (Carleman estimate in 1D). *There exists a constant $\beta_0 > 0$ such that for every $\beta \geq \beta_0$ there exists $\lambda_0 > 0$ (depending on L, v_0 , and β) with the following property: for all $\lambda \geq \lambda_0$ and all $u \in C^2([0, L])$, one has the pointwise estimate*

$$r(v)^{\beta+2} e^{2\lambda r(v)^{-\beta}} |u''(v)|^2 \geq C \left(U'(v) + \lambda^3 \beta^4 e^{2\lambda r(v)^{-\beta}} r(v)^{-2\beta-2} |u(v)|^2 + \lambda \beta e^{2\lambda r(v)^{-\beta}} |u'(v)|^2 \right), \quad (2.1)$$

for $v \in (0, L)$, where $C > 0$ is independent of u and (λ, β) , and the auxiliary function U satisfies

$$|U(v)| \leq C e^{2\lambda r(v)^{-\beta}} \left(\lambda^3 \beta^3 r(v)^{-2\beta-2} |u(v)|^2 + \lambda \beta |u'(v)|^2 \right), \quad v \in (0, L). \quad (2.2)$$

Remark 1. *The estimate in Lemma 1 is the 1D counterpart of the piecewise Carleman estimate established in [29, Section 3] (corresponding to the case $d = 1$ and $A \equiv 1$). For this reason, we omit the proof and refer the reader to that reference.*

Integrating (2.1) over $[0, L]$ and using (2.2), we obtain the following integrated form, which includes boundary terms at $v = 0$ and $v = L$.

Corollary 1 (Integrated Carleman estimate). *Under the assumptions of Lemma 1, there exists $C > 0$ such that*

$$\int_0^L e^{2\lambda r(v)^{-\beta}} |u''(v)|^2 dv \geq C \int_0^L e^{2\lambda r(v)^{-\beta}} \left(\lambda^3 |u(v)|^2 + \lambda |u'(v)|^2 \right) dv - C \sum_{\xi \in \{0, L\}} e^{2\lambda r(\xi)^{-\beta}} \left(\lambda^3 |u(\xi)|^2 + \lambda |u'(\xi)|^2 \right). \quad (2.3)$$

In particular, if $u(0) = u(L) = u'(0) = u'(L) = 0$, then the boundary contribution in (2.3) vanishes.

2.2 The Legendre polynomial–exponential basis

The Legendre polynomial–exponential basis, first introduced in [15], is fundamental to the time-dimensional reduction method employed in this study. This basis combines the spectral structure of the classical Legendre polynomials with an exponential weight, yielding an orthonormal system in an exponentially weighted Hilbert space. For the reader’s convenience, we briefly summarize the main definitions and properties below.

Let $\{P_n\}_{n \geq 0}$ denote the Legendre polynomials on $(-1, 1)$, defined by Rodrigues’ formula

$$P_n(x) = \frac{1}{2^n n!} \frac{d^n}{dx^n} (x^2 - 1)^n.$$

Using the affine transformation

$$x = \frac{2t}{T} - 1, \quad t \in (0, T),$$

we define the rescaled polynomials

$$Q_n(t) := \sqrt{\frac{2n+1}{T}} P_n\left(\frac{2t}{T} - 1\right), \quad t \in (0, T).$$

The family $\{Q_n\}_{n \geq 0}$ forms an orthonormal basis of $L^2(0, T)$. We then define the Legendre polynomial–exponential basis by

$$\Psi_n(t) := e^t Q_n(t), \quad t \in (0, T), \quad n \geq 0.$$

The system $\{\Psi_n\}_{n \geq 0}$ forms an orthonormal basis of $L^2(0, T)$ with respect to the inner product

$$\langle u, v \rangle_{e^{-2t}} := \int_0^T e^{-2t} u(t) v(t) dt.$$

Proposition 1 (See [15]). *The Legendre polynomial–exponential basis functions Ψ_n , $n \geq 0$, satisfy the following properties.*

1. For each $n \geq 0$, the function Ψ_n is infinitely differentiable on $(0, T)$, and none of its derivatives of any order vanishes identically on this interval.
2. For every integer $\ell \in \mathbb{N}$, there exists a constant $C > 0$, depending only on ℓ and T , such that for all $u \in H^\ell(0, T)$,

$$\sum_{n=0}^{\infty} n^{2\ell} |\langle u, \Psi_n \rangle_{e^{-2t}}|^2 \leq C \|u\|_{H^\ell(0, T)}^2. \quad (2.4)$$

3. There exists a constant $C > 0$, depending only on T , such that for all $n \geq 1$,

$$\|\Psi'_n\|_{e^{-2t}} \leq C n^{3/2}. \quad (2.5)$$

Remark 2 (The role of the weight e^t). *We omit the proof of Proposition 1, since it follows from Proposition 2.1, Lemma 2.1, and the first part of Lemma 2.2 in [15]. The exponential factor e^t in the definition $\Psi_n = e^t Q_n$ plays a crucial role. Without this weight, some derivatives of the time basis functions may vanish identically; for instance, this happens for the constant mode. See item 2 of Remark 7 for the significance of this property in our numerical method.*

The following proposition is the one-derivative analogue of the convergence result proved in [15] for the second derivative.

Proposition 2. *Let $p \geq 0$ and assume that*

$$u \in H^\ell((0, T); H^p(0, L)) \quad \text{for some } \ell \geq 3.$$

Denote the Legendre–exponential coefficients of u by

$$u_n(\cdot) := \langle u(\cdot, \cdot), \Psi_n \rangle_{L^2_{e^{-2t}}(0, T)} = \int_0^T e^{-2t} u(\cdot, t) \Psi_n(t) dt, \quad n \geq 0.$$

Then $u_t \in L^2((0, T); H^p(0, L))$ and

$$\partial_t u(\cdot, t) = \sum_{n=0}^{\infty} u_n(\cdot) \Psi'_n(t) \quad \text{in } L^2((0, T); H^p(0, L)).$$

Remark 3. *The proof of Proposition 2 follows the same arguments as the proof of the second-derivative result in [15]. The threshold $\ell \geq 3$ arises from combining the coefficient decay estimate (2.4) with the derivative bound (2.5), see [49, Theorem 1] for more details.*

2.3 Some Lipschitz continuities

Let N be a cutoff number and let $\{\Psi_n\}_{n=0}^N$ be the first $N + 1$ elements of the Legendre–exponential basis introduced above. To simplify notation, we introduce the projected operator in the coefficient space.

Definition 1 (The projected collision operators). *For $\mathbf{f} = [f_0 \ \dots \ f_N]^\top \in [H^3(0, \infty)]^{N+1}$, define, for each $m = 0, \dots, N$ and $v \in (0, \infty)$,*

$$\begin{aligned} Q_{\text{coag}, m}(\mathbf{f})(v) &:= \int_0^T Q_{\text{coag}} \left(\sum_{n=0}^N f_n(v) \Psi_n(t) \right) e^{-2t} \Psi_m(t) dt, \\ Q_{\text{frag}, m}(\mathbf{f})(v) &:= \int_0^T Q_{\text{frag}} \left(\sum_{n=0}^N f_n(v) \Psi_n(t) \right) e^{-2t} \Psi_m(t) dt, \\ Q_m(\mathbf{f})(v) &:= Q_{\text{coag}, m}(\mathbf{f})(v) + Q_{\text{frag}, m}(\mathbf{f})(v). \end{aligned}$$

In vector form, we write

$$\mathbf{Q}_{\text{coag}}(\mathbf{f})(v) := \begin{bmatrix} Q_{\text{coag}, 0}(\mathbf{f})(v) \\ \vdots \\ Q_{\text{coag}, N}(\mathbf{f})(v) \end{bmatrix}, \quad \mathbf{Q}_{\text{frag}}(\mathbf{f})(v) := \begin{bmatrix} Q_{\text{frag}, 0}(\mathbf{f})(v) \\ \vdots \\ Q_{\text{frag}, N}(\mathbf{f})(v) \end{bmatrix}, \quad \mathbf{Q}(\mathbf{f})(v) := \begin{bmatrix} Q_0(\mathbf{f})(v) \\ \vdots \\ Q_N(\mathbf{f})(v) \end{bmatrix},$$

for all $v \in [0, \infty)$.

In Definition 1, the projected operators $Q_{\text{coag}, m}(\mathbf{f})$, $Q_{\text{frag}, m}(\mathbf{f})$, and $Q_m(\mathbf{f})$ are defined for coefficient vectors

$$\mathbf{f} \in [H^3(0, \infty)]^{N+1}.$$

However, in our inverse problem, the unknown coefficient vector \mathbf{f} is sought only on the computational interval $(0, L)$. Therefore, in order to evaluate these projected operators for $v \in (0, L)$, we must extend \mathbf{f} from $(0, L)$ to $(0, \infty)$.

Remark 4. Note that, when numerically solving coagulation–fragmentation models [16, 20, 47], and more generally kinetic equations posed on the full space [20, 21, 23], it is necessary to truncate the computational domain to a bounded interval. Accordingly, in the inverse problem considered above, the observation domain in v is restricted from $(0, \infty)$ to $(0, L)$. Owing to this truncation, the measurements may contain noise near the boundary. Our method, however, remains robust to such boundary perturbations, and noisy boundary data does not pose any essential difficulty for the numerical results.

Remark 5 (Exponential tail extension). Throughout this subsection, whenever a coefficient vector

$$\mathbf{f} = [f_0 \quad \dots \quad f_N]^\top$$

is only prescribed on $(0, L)$, we extend each component to $(0, \infty)$ by

$$f_n(v) := f_n(L)e^{-(v-L)}, \quad v \geq L, \quad n = 0, \dots, N. \quad (2.6)$$

All occurrences of $Q_{\text{coag},m}(\mathbf{f})$, $Q_{\text{frag},m}(\mathbf{f})$, and $Q_m(\mathbf{f})$ in this subsection are understood with this extension.

To control the nonlinear projected operators defined in Definition 1 and to obtain uniform estimates in the subsequent analysis, we restrict attention to coefficient vectors that satisfy an a priori bound. Such a restriction is standard in nonlinear inverse problems and allows the Lipschitz constants in our estimates to depend only on the prescribed bound. We therefore introduce the following admissible set.

Definition 2 (Admissible set). Let $M \gg 1$ be a prescribed number. Define

$$B := \left\{ \mathbf{f} \in [H^3(0, L)]^{N+1} : \|\mathbf{f}\|_{[L^2(0, L)]^{N+1}} + \|\mathbf{f}\|_{[L^\infty(0, L)]^{N+1}} \leq M \right\}.$$

Assumption 1 (Coefficient conditions). The kernels K and V are continuous functions that satisfy

$$\sup_{v \in (0, L)} \int_0^\infty K(v, v^*)^2 e^{-2(v^*-L)_+} dv^* < \infty, \quad \sup_{v \in (0, L)} \int_0^\infty V(v, v^*)^2 e^{-2v^*} dv^* < \infty, \quad (2.7)$$

and

$$\sup_{v \in (0, L)} \int_0^\infty K(v, v^*) e^{-(v^*-L)_+} dv^* < \infty, \quad \sup_{v \in (0, L)} \int_0^\infty V(v, v^*) e^{-v^*} dv^* < \infty. \quad (2.8)$$

In addition, K and V are symmetric, that is,

$$K(v^*, v) = K(v, v^*) \quad \text{and} \quad V(v^*, v) = V(v, v^*) \quad \text{for all } v, v^* \geq 0.$$

Moreover, $b \in L^\infty(0, \infty)$.

Remark 6. Some examples of K are given below:

- (i) $K(v, v^*) = c_K(v + v^*)^a$, where $c_K > 0$ and $a \geq 0$.
- (ii) $K(v, v^*) = c_K(v^a + (v^*)^a)$, where $c_K > 0$ and $a \geq 0$.
- (iii) $K(v, v^*) = c_K(v + v^*)^a(v^b + (v^*)^b)$, where $c_K > 0$ and $a, b \geq 0$.
- (iv) $K(v, v^*) = c_K(v^a + (v^*)^a)(v^b + (v^*)^b)$, where $c_K > 0$ and $a, b \geq 0$.
- (v) $K(v, v^*) = c_K(v^a(v^*)^b + (v^*)^a v^b)$, where $c_K > 0$ and $a, b \geq 0$.

Analogous choices can also be made for V .

Since V is symmetric, (2.8) implies

$$\sup_{v \in (0, L)} \int_0^v V(v - v^*, v) dv^* < \infty. \quad (2.9)$$

In fact, since V is symmetric, we have

$$V(v - v^*, v) = V(v, v - v^*).$$

Therefore, by the change of variable $s = v - v^*$,

$$\int_0^v V(v - v^*, v) dv^* = \int_0^v V(v, s) ds.$$

Because $0 < s < v < L$, it follows that $e^{-s} \geq e^{-L}$, and hence

$$\int_0^v V(v, s) ds \leq e^L \int_0^v V(v, s) e^{-s} ds \leq e^L \int_0^\infty V(v, s) e^{-s} ds.$$

Taking the supremum over $v \in (0, L)$ and using (2.8), we obtain (2.9).

These conditions are compatible with polynomial-type kernels because of the exponential tail (2.6).

Lemma 2 (Lipschitz continuity of $Q_{\text{coag},m}$ on B). *Suppose that all conditions in Assumption 1 hold. Then for each $m = 0, \dots, N$ there exists a constant $C > 0$, depending only on $M, \{\Psi_n\}_{n=0}^N, T, K$, and L , such that for all $\mathbf{f}, \mathbf{g} \in B$,*

$$\begin{aligned} \int_0^L e^{2\lambda r(v)^{-\beta}} |Q_{\text{coag},m}(\mathbf{f})(v) - Q_{\text{coag},m}(\mathbf{g})(v)|^2 dv \\ \leq C \int_0^L e^{2\lambda r(v)^{-\beta}} |\mathbf{f}(v) - \mathbf{g}(v)|^2 dv + C e^{2\lambda r(L)^{-\beta}} |\mathbf{f}(L) - \mathbf{g}(L)|^2. \end{aligned} \quad (2.10)$$

Proof. We define

$$\mathcal{F}(v, t) := \sum_{n=0}^N f_n(v) \Psi_n(t), \quad \mathcal{G}(v, t) := \sum_{n=0}^N g_n(v) \Psi_n(t), \quad \mathcal{H} := \mathcal{F} - \mathcal{G}.$$

Since N is fixed and $\Psi_0, \dots, \Psi_N \in C([0, T])$, there exists a constant $C > 0$, depending only on $\{\Psi_n\}_{n=0}^N$ and T , such that

$$|\mathcal{F}(v, t)| + |\mathcal{G}(v, t)| \leq CM, \quad (v, t) \in (0, L) \times (0, T), \quad (2.11)$$

for all $\mathbf{f}, \mathbf{g} \in B$. Moreover, by extension (2.6),

$$|\mathcal{F}(v, t)| + |\mathcal{G}(v, t)| \leq CM e^{-(v-L)}, \quad v > L, t \in (0, T). \quad (2.12)$$

Using the orthonormality of $\{\Psi_n\}_{n=0}^N$ in $L^2_{e^{-2t}}(0, T)$, we also have

$$\int_0^T e^{-2t} |\mathcal{H}(v, t)|^2 dt = \begin{cases} |\mathbf{f}(v) - \mathbf{g}(v)|^2, & 0 < v < L, \\ e^{-2(v-L)} |\mathbf{f}(L) - \mathbf{g}(L)|^2, & v \geq L. \end{cases} \quad (2.13)$$

For each $m = 0, \dots, N$, write

$$Q_{\text{coag},m}(\mathbf{f})(v) - Q_{\text{coag},m}(\mathbf{g})(v) = I_m^{(1)}(v) - I_m^{(2)}(v),$$

where

$$\begin{aligned} I_m^{(1)}(v) &:= \frac{1}{2} \int_0^T \int_0^v K(v - v^*, v^*) \left(\mathcal{F}(v - v^*, t) \mathcal{F}(v^*, t) - \mathcal{G}(v - v^*, t) \mathcal{G}(v^*, t) \right) e^{-2t} \Psi_m(t) dv^* dt, \\ I_m^{(2)}(v) &:= \int_0^T \left(\mathcal{F}(v, t) \int_0^\infty K(v, v^*) \mathcal{F}(v^*, t) dv^* - \mathcal{G}(v, t) \int_0^\infty K(v, v^*) \mathcal{G}(v^*, t) dv^* \right) e^{-2t} \Psi_m(t) dt. \end{aligned}$$

Hence,

$$|Q_{\text{coag},m}(\mathbf{f})(v) - Q_{\text{coag},m}(\mathbf{g})(v)|^2 \leq 2|I_m^{(1)}(v)|^2 + 2|I_m^{(2)}(v)|^2. \quad (2.14)$$

Step 1: Estimate of the first term. Using

$$\mathcal{F}(v - v^*, t)\mathcal{F}(v^*, t) - \mathcal{G}(v - v^*, t)\mathcal{G}(v^*, t) = \mathcal{H}(v - v^*, t)\mathcal{F}(v^*, t) + \mathcal{G}(v - v^*, t)\mathcal{H}(v^*, t),$$

Cauchy–Schwarz in t , and $\|\Psi_m\|_{L^2_{e^{-2t}}(0, T)} = 1$, we obtain

$$\begin{aligned} |I_m^{(1)}(v)|^2 &\leq C \int_0^T e^{-2t} \left| \int_0^v K(v - v^*, v^*) \left(\mathcal{H}(v - v^*, t)\mathcal{F}(v^*, t) + \mathcal{G}(v - v^*, t)\mathcal{H}(v^*, t) \right) dv^* \right|^2 dt \\ &\leq C \int_0^T e^{-2t} \left[\left(\int_0^v K(v - v^*, v^*) |\mathcal{H}(v - v^*, t)| dv^* \right)^2 \right. \\ &\quad \left. + \left(\int_0^v K(v - v^*, v^*) |\mathcal{H}(v^*, t)| dv^* \right)^2 \right] dt, \end{aligned} \quad (2.15)$$

where we used (2.11). Since $v \in (0, L)$, both variables in this integral stay in $(0, L)$, and (2.7) implies

$$\sup_{x \in (0, L)} \int_0^L K(x, y)^2 dy < \infty.$$

Therefore, by the Cauchy–Schwarz inequality with respect to the variable v^* ,

$$\left(\int_0^v K(v - v^*, v^*) |\mathcal{H}(v - v^*, t)| dv^* \right)^2 \leq C \int_0^v |\mathcal{H}(s, t)|^2 ds,$$

and similarly,

$$\left(\int_0^v K(v - v^*, v^*) |\mathcal{H}(v^*, t)| dv^* \right)^2 \leq C \int_0^v |\mathcal{H}(s, t)|^2 ds.$$

Here we denote $C > 0$ as a constant depending only on $\{\Psi_n\}_{n=0}^N$ and T , that varies from line to line. Substituting these bounds into (2.15) and then using (2.13), we get

$$|I_m^{(1)}(v)|^2 \leq C \int_0^v |\mathbf{f}(s) - \mathbf{g}(s)|^2 ds, \quad v \in (0, L). \quad (2.16)$$

Since $r(v) = v - v_0$ is increasing, the Carleman weight $e^{2\lambda r(v)^{-\beta}}$ is decreasing on $[0, L]$. Hence, by Fubini's theorem and (2.16),

$$\begin{aligned} \int_0^L e^{2\lambda r(v)^{-\beta}} |I_m^{(1)}(v)|^2 dv &\leq C \int_0^L e^{2\lambda r(v)^{-\beta}} \int_0^v |\mathbf{f}(s) - \mathbf{g}(s)|^2 ds dv \\ &= C \int_0^L \left(\int_s^L e^{2\lambda r(v)^{-\beta}} dv \right) |\mathbf{f}(s) - \mathbf{g}(s)|^2 ds \\ &\leq CL \int_0^L e^{2\lambda r(s)^{-\beta}} |\mathbf{f}(s) - \mathbf{g}(s)|^2 ds. \end{aligned} \quad (2.17)$$

Step 2: Estimate of the second term. We write

$$I_m^{(2)}(v) = J_{m,1}(v) + J_{m,2}(v),$$

where

$$\begin{aligned} J_{m,1}(v) &:= \int_0^T \mathcal{H}(v, t) \left(\int_0^\infty K(v, v^*) \mathcal{F}(v^*, t) dv^* \right) e^{-2t} \Psi_m(t) dt, \\ J_{m,2}(v) &:= \int_0^T \mathcal{G}(v, t) \left(\int_0^\infty K(v, v^*) \mathcal{H}(v^*, t) dv^* \right) e^{-2t} \Psi_m(t) dt. \end{aligned}$$

We first bound the inner factor in $J_{m,1}$. To this end, we split the v^* -integral into $(0, L)$ and (L, ∞) . On $(0, L)$, using (2.11) and (2.7),

$$\int_0^L K(v, v^*) |\mathcal{F}(v^*, t)| dv^* \leq CM \left(\int_0^L K(v, v^*)^2 dv^* \right)^{1/2} \leq C.$$

Here, again, we denote $C > 0$ as a constant depending only on $\{\Psi_n\}_{n=0}^N$ and T , that varies from line to line. On (L, ∞) , (2.12) and the additional tail bound on K yield

$$\int_L^\infty K(v, v^*) |\mathcal{F}(v^*, t)| dv^* \leq CM \int_L^\infty K(v, v^*) e^{-(v^*-L)} dv^* \leq C.$$

Hence,

$$\sup_{(v,t) \in (0,L) \times (0,T)} \left| \int_0^\infty K(v, v^*) \mathcal{F}(v^*, t) dv^* \right| \leq C. \quad (2.18)$$

Using (2.18), the Cauchy–Schwarz inequality with respect to t , and (2.13), we obtain

$$|J_{m,1}(v)|^2 \leq C \int_0^T e^{-2t} |\mathcal{H}(v, t)|^2 dt = C |\mathbf{f}(v) - \mathbf{g}(v)|^2, \quad v \in (0, L).$$

Therefore,

$$\int_0^L e^{2\lambda r(v)^{-\beta}} |J_{m,1}(v)|^2 dv \leq C \int_0^L e^{2\lambda r(v)^{-\beta}} |\mathbf{f}(v) - \mathbf{g}(v)|^2 dv. \quad (2.19)$$

We next treat $J_{m,2}$. Again, we split the v^* -integral into $(0, L)$ and (L, ∞) . By (2.7) and the Cauchy–Schwarz inequality,

$$\int_0^L K(v, v^*) |\mathcal{H}(v^*, t)| dv^* \leq C \left(\int_0^L |\mathcal{H}(v^*, t)|^2 dv^* \right)^{1/2}.$$

Using the tail extension and the additional tail bound on K , we get

$$\int_L^\infty K(v, v^*) |\mathcal{H}(v^*, t)| dv^* \leq C |\mathbf{f}(L) - \mathbf{g}(L)|.$$

Thus,

$$\left| \int_0^\infty K(v, v^*) \mathcal{H}(v^*, t) dv^* \right| \leq C \left(\|\mathcal{H}(\cdot, t)\|_{L^2(0,L)} + |\mathbf{f}(L) - \mathbf{g}(L)| \right).$$

Combining this with (2.11) and the Cauchy–Schwarz inequality in t , we get

$$\begin{aligned} |J_{m,2}(v)|^2 &\leq C \int_0^T e^{-2t} \left(\|\mathcal{H}(\cdot, t)\|_{L^2(0,L)}^2 + |\mathbf{f}(L) - \mathbf{g}(L)|^2 \right) dt \\ &\leq C \int_0^L |\mathbf{f}(s) - \mathbf{g}(s)|^2 ds + C |\mathbf{f}(L) - \mathbf{g}(L)|^2. \end{aligned} \quad (2.20)$$

Since $e^{2\lambda r(v)^{-\beta}}$ is decreasing on $[0, L]$, (2.20) implies

$$\begin{aligned} \int_0^L e^{2\lambda r(v)^{-\beta}} |J_{m,2}(v)|^2 dv &\leq C \int_0^L e^{2\lambda r(v)^{-\beta}} dv \int_0^L |\mathbf{f}(s) - \mathbf{g}(s)|^2 ds \\ &\quad + C \int_0^L e^{2\lambda r(v)^{-\beta}} dv |\mathbf{f}(L) - \mathbf{g}(L)|^2 \\ &\leq C \int_0^L e^{2\lambda r(s)^{-\beta}} |\mathbf{f}(s) - \mathbf{g}(s)|^2 ds + C e^{2\lambda r(L)^{-\beta}} |\mathbf{f}(L) - \mathbf{g}(L)|^2. \end{aligned} \quad (2.21)$$

Here, the constant $C > 0$ depends on $\{\Psi_n\}_{n=0}^N$ and T and also on L .

Combining (2.19) and (2.21), we obtain

$$\int_0^L e^{2\lambda r(v)^{-\beta}} |I_m^{(2)}(v)|^2 dv \leq C \int_0^L e^{2\lambda r(v)^{-\beta}} |\mathbf{f}(v) - \mathbf{g}(v)|^2 dv + C e^{2\lambda r(L)^{-\beta}} |\mathbf{f}(L) - \mathbf{g}(L)|^2. \quad (2.22)$$

Step 3: Conclusion. Finally, (2.14), (2.17), and (2.22) yield (2.10). \square

Lemma 3 (Lipschitz continuity of $Q_{\text{frag},m}$ on B). *Suppose that all conditions in Assumption 1 hold. Then for each $m = 0, \dots, N$ there exists a constant $C > 0$, depending only on $\{\Psi_n\}_{n=0}^N$, T , V , and L (and the extension (2.6)), such that for all $\mathbf{f}, \mathbf{g} \in B$,*

$$\begin{aligned} \int_0^L e^{2\lambda r(v)^{-\beta}} |Q_{\text{frag},m}(\mathbf{f})(v) - Q_{\text{frag},m}(\mathbf{g})(v)|^2 dv \\ \leq C \int_0^L e^{2\lambda r(v)^{-\beta}} |\mathbf{f}(v) - \mathbf{g}(v)|^2 dv + C e^{2\lambda r(L)^{-\beta}} |\mathbf{f}(L) - \mathbf{g}(L)|^2. \end{aligned} \quad (2.23)$$

Proof. Let \mathcal{F} , \mathcal{G} , and \mathcal{H} be as in the proof of Lemma 2. In particular,

$$\int_0^T e^{-2t} |\mathcal{H}(v, t)|^2 dt = \begin{cases} |\mathbf{f}(v) - \mathbf{g}(v)|^2, & v \in (0, L), \\ e^{-2(v-L)} |\mathbf{f}(L) - \mathbf{g}(L)|^2, & v > L, \end{cases}$$

where for $v > L$ we use the extension (2.6).

Since Q_{frag} is linear, we have

$$Q_{\text{frag},m}(\mathbf{f})(v) - Q_{\text{frag},m}(\mathbf{g})(v) = \int_0^T Q_{\text{frag}}(\mathcal{H})(v, t) e^{-2t} \Psi_m(t) dt.$$

By (1.4),

$$Q_{\text{frag}}(\mathcal{H})(v, t) = -\mathcal{H}(v, t) \int_0^v V(v - v^*, v) dv^* + 2 \int_0^\infty V(v, v^*) \mathcal{H}(v + v^*, t) dv^*.$$

Therefore,

$$Q_{\text{frag},m}(\mathbf{f})(v) - Q_{\text{frag},m}(\mathbf{g})(v) = J_m^{(1)}(v) + J_m^{(2)}(v),$$

where

$$\begin{aligned} J_m^{(1)}(v) &:= - \int_0^T \mathcal{H}(v, t) \left(\int_0^v V(v - v^*, v) dv^* \right) e^{-2t} \Psi_m(t) dt, \\ J_m^{(2)}(v) &:= 2 \int_0^T \left(\int_0^\infty V(v, v^*) \mathcal{H}(v + v^*, t) dv^* \right) e^{-2t} \Psi_m(t) dt. \end{aligned}$$

Hence,

$$|Q_{\text{frag},m}(\mathbf{f})(v) - Q_{\text{frag},m}(\mathbf{g})(v)|^2 \leq 2|J_m^{(1)}(v)|^2 + 2|J_m^{(2)}(v)|^2. \quad (2.24)$$

For the first term, by the Cauchy–Schwarz inequality in t , $\|\Psi_m\|_{L_{e^{-2t}}(0, T)} = 1$, and (2.9),

$$|J_m^{(1)}(v)|^2 \leq \left(\int_0^v V(v - v^*, v) dv^* \right)^2 \int_0^T e^{-2t} |\mathcal{H}(v, t)|^2 dt \leq C |\mathbf{f}(v) - \mathbf{g}(v)|^2,$$

for all $v \in (0, L)$. Thus,

$$\int_0^L e^{2\lambda r(v)^{-\beta}} |J_m^{(1)}(v)|^2 dv \leq C \int_0^L e^{2\lambda r(v)^{-\beta}} |\mathbf{f}(v) - \mathbf{g}(v)|^2 dv. \quad (2.25)$$

We next estimate the second term. For fixed $v \in (0, L)$, split

$$\int_0^\infty V(v, v^*) \mathcal{H}(v + v^*, t) dv^* = \int_0^{L-v} V(v, v^*) \mathcal{H}(v + v^*, t) dv^* + \int_{L-v}^\infty V(v, v^*) \mathcal{H}(v + v^*, t) dv^*.$$

For the first part, since $v + v^* \in (0, L)$ when $0 < v^* < L - v$, the Cauchy–Schwarz inequality and (2.7) give

$$\left| \int_0^{L-v} V(v, v^*) \mathcal{H}(v + v^*, t) dv^* \right|^2 \leq C \int_v^L |\mathcal{H}(s, t)|^2 ds.$$

Here, again, we denote $C > 0$ as a constant depending only on $\{\Psi_n\}_{n=0}^N, V, L$ and T , that varies from line to line. For the second part, using the extension (2.6), we arrive at

$$\mathcal{H}(v + v^*, t) = \mathcal{H}(L, t)e^{-(v+v^*-L)}, \quad v^* > L - v,$$

and therefore

$$\begin{aligned} \left| \int_{L-v}^{\infty} V(v, v^*) \mathcal{H}(v + v^*, t) dv^* \right| &\leq |\mathcal{H}(L, t)| \int_{L-v}^{\infty} V(v, v^*) e^{-(v+v^*-L)} dv^* \\ &\leq C |\mathcal{H}(L, t)|, \end{aligned}$$

where in the last step we used (2.8).

Combining the two parts, we find

$$\left| \int_0^{\infty} V(v, v^*) \mathcal{H}(v + v^*, t) dv^* \right|^2 \leq C \int_v^L |\mathcal{H}(s, t)|^2 ds + C |\mathcal{H}(L, t)|^2.$$

Applying the Cauchy–Schwarz inequality in t again yields

$$|J_m^{(2)}(v)|^2 \leq C \int_0^T e^{-2t} \int_v^L |\mathcal{H}(s, t)|^2 ds dt + C \int_0^T e^{-2t} |\mathcal{H}(L, t)|^2 dt.$$

Therefore,

$$|J_m^{(2)}(v)|^2 \leq C \int_v^L |\mathbf{f}(s) - \mathbf{g}(s)|^2 ds + C |\mathbf{f}(L) - \mathbf{g}(L)|^2.$$

Multiplying both sides of the above inequality by $e^{2\lambda r(v)^{-\beta}}$, integrating over $(0, L)$, and using Fubini's theorem together with the monotonicity of $e^{2\lambda r(v)^{-\beta}}$, we obtain

$$\begin{aligned} \int_0^L e^{2\lambda r(v)^{-\beta}} |J_m^{(2)}(v)|^2 dv &\leq C \int_0^L e^{2\lambda r(v)^{-\beta}} \int_v^L |\mathbf{f}(s) - \mathbf{g}(s)|^2 ds dv + C \int_0^L e^{2\lambda r(v)^{-\beta}} dv |\mathbf{f}(L) - \mathbf{g}(L)|^2 \\ &\leq C \int_0^L e^{2\lambda r(v)^{-\beta}} |\mathbf{f}(v) - \mathbf{g}(v)|^2 dv + C e^{2\lambda r(L)^{-\beta}} |\mathbf{f}(L) - \mathbf{g}(L)|^2. \end{aligned} \quad (2.26)$$

Finally, (2.24), (2.25), and (2.26) imply (2.23). \square

Lemma 4 (Lipschitz continuity of Q_m on B). *Assume Assumption 1. Then, for each $m = 0, \dots, N$, there exists a constant $C > 0$, depending only on $M, \{\Psi_n\}_{n=0}^N, T, K, V$, and L , such that for all $\mathbf{f}, \mathbf{g} \in B$,*

$$\begin{aligned} \int_0^L e^{2\lambda r(v)^{-\beta}} |Q_m(\mathbf{f})(v) - Q_m(\mathbf{g})(v)|^2 dv \\ \leq C \int_0^L e^{2\lambda r(v)^{-\beta}} |\mathbf{f}(v) - \mathbf{g}(v)|^2 dv + C e^{2\lambda r(L)^{-\beta}} |\mathbf{f}(L) - \mathbf{g}(L)|^2. \end{aligned} \quad (2.27)$$

Proof. By Definition 1,

$$Q_m(\mathbf{f})(v) - Q_m(\mathbf{g})(v) = \left(Q_{\text{coag},m}(\mathbf{f})(v) - Q_{\text{coag},m}(\mathbf{g})(v) \right) + \left(Q_{\text{frag},m}(\mathbf{f})(v) - Q_{\text{frag},m}(\mathbf{g})(v) \right).$$

Hence, by the elementary inequality $|a + b|^2 \leq 2|a|^2 + 2|b|^2$,

$$\begin{aligned} |Q_m(\mathbf{f})(v) - Q_m(\mathbf{g})(v)|^2 &\leq 2|Q_{\text{coag},m}(\mathbf{f})(v) - Q_{\text{coag},m}(\mathbf{g})(v)|^2 \\ &\quad + 2|Q_{\text{frag},m}(\mathbf{f})(v) - Q_{\text{frag},m}(\mathbf{g})(v)|^2. \end{aligned}$$

Multiplying by $e^{2\lambda r(v)^{-\beta}}$ and integrating over $(0, L)$, we obtain

$$\begin{aligned} & \int_0^L e^{2\lambda r(v)^{-\beta}} |Q_m(\mathbf{f})(v) - Q_m(\mathbf{g})(v)|^2 dv \\ & \leq 2 \int_0^L e^{2\lambda r(v)^{-\beta}} |Q_{\text{coag},m}(\mathbf{f})(v) - Q_{\text{coag},m}(\mathbf{g})(v)|^2 dv \\ & \quad + 2 \int_0^L e^{2\lambda r(v)^{-\beta}} |Q_{\text{frag},m}(\mathbf{f})(v) - Q_{\text{frag},m}(\mathbf{g})(v)|^2 dv. \end{aligned}$$

Applying Lemmas 2 and 3, and enlarging the constant if necessary, we obtain (2.27). \square

3 Time-dimension reduction

In this section, we eliminate the time variable by expanding the solution $f(v, t)$ in a truncated Legendre–exponential basis with respect to t . This procedure transforms the original time-dependent inverse problem into a coupled time-independent system for the expansion coefficients of f .

Let $\{\Psi_n(t)\}_{n=0}^\infty$ be the Legendre–exponential basis on $[0, T]$ defined as in Section 2.2. We expand f as

$$f(v, t) = \sum_{n=0}^\infty f_n(v) \Psi_n(t), \quad (v, t) \in (0, \infty) \times (0, T), \quad (3.1)$$

where

$$f_n(v) = \int_0^T e^{-2t} f(v, t) \Psi_n(t) dt, \quad v \in (0, \infty).$$

Substituting (3.1) into the governing equation (1.1), we obtain

$$f_t(v, t) = -b(v) \sum_{n=0}^\infty f'_n(v) \Psi_n(t) + \sum_{n=0}^\infty f''_n(v) \Psi_n(t) + Q \left(\sum_{n=0}^\infty f_n(v) \Psi_n(t) \right), \quad (3.2)$$

where Q is the coagulation–fragmentation operator defined in (1.2), (1.3), and (1.4).

Under the regularity assumption of Proposition 2, we may differentiate the expansion (3.1) term-by-term in t . Therefore, (3.2) can be rewritten as

$$\sum_{n=0}^\infty f_n(v) \Psi'_n(t) = -b(v) \sum_{n=0}^\infty f'_n(v) \Psi_n(t) + \sum_{n=0}^\infty f''_n(v) \Psi_n(t) + Q \left(\sum_{n=0}^\infty f_n(v) \Psi_n(t) \right), \quad (3.3)$$

for $(v, t) \in (0, L) \times (0, T)$, where the series converge in $L^2_{e^{-2t}}((0, T); L^2(0, L))$.

Accordingly, (3.3) is approximated by

$$\sum_{n=0}^N f_n(v) \Psi'_n(t) = -b(v) \sum_{n=0}^N f'_n(v) \Psi_n(t) + \sum_{n=0}^N f''_n(v) \Psi_n(t) + Q \left(\sum_{n=0}^N f_n(v) \Psi_n(t) \right), \quad (3.4)$$

for $(v, t) \in (0, \infty) \times (0, T)$, where N is a cutoff number chosen later in the numerical study.

For each $m \in \{0, 1, \dots, N\}$, multiply both sides of (3.4) by $e^{-2t} \Psi_m(t)$ and integrate over $(0, T)$. Using the orthonormality

$$\int_0^T e^{-2t} \Psi_n(t) \Psi_m(t) dt = \delta_{mn},$$

we obtain

$$-f''_m(v) + b(v) f'_m(v) + \sum_{n=0}^N s_{mn} f_n(v) = \int_0^T Q \left(\sum_{n=0}^N f_n(v) \Psi_n(t) \right) e^{-2t} \Psi_m(t) dt, \quad (3.5)$$

for $v \in (0, \infty)$, where

$$s_{mn} := \int_0^T e^{-2t} \Psi'_n(t) \Psi_m(t) dt.$$

To solve the inverse problem stated in Problem 1, we restrict (3.5) to the computational domain $(0, L)$ and use Definition 1 to write

$$-f''_m(v) + b(v)f'_m(v) + \sum_{n=0}^N s_{mn} f_n(v) = Q_m(\mathbf{f}^N)(v), \quad v \in (0, L). \quad (3.6)$$

Remark 7. Equation (3.6) is a central ingredient of our numerical method. Its derivation relies on truncating the Fourier expansion of f with respect to the Legendre–exponential basis $\{\Psi_n\}_{n \geq 0}$. A natural question is why this particular basis is chosen among the many orthonormal bases of $L^2(0, T)$. The reasons are as follows.

1. In the derivation of (3.5), we need Proposition 2 in order to represent the time derivative in the form

$$f_t(v, t) = \sum_{n=0}^{\infty} f_n(v) \Psi'_n(t),$$

as in (3.3). This property may fail for other choices of orthonormal bases.

2. Another important requirement is that no basis function should have identically vanishing derivative. Indeed, if there exists an index n_0 such that

$$\Psi'_{n_0}(t) = 0 \quad \text{for all } t \in (0, T),$$

Then the corresponding Fourier mode f_{n_0} would disappear from the left-hand side of (3.3), thereby reducing the accuracy of the numerical method. This issue occurs, for example, for the classical Legendre polynomial basis and the standard trigonometric Fourier basis, whose first basis element is constant. In such cases, the mode $f_0(v)$ does not contribute to the equation for f_t . By contrast, the Legendre–exponential basis avoids this difficulty; see Remark 2. We also refer the reader to [49, Figures 3 and 4], where the reconstruction of the initial data for the compressible anisotropic Navier–Stokes equation is compared with and without the exponential weight in the basis. Those numerical results show that the Legendre–exponential basis leads to significantly better reconstructions, whereas the classical Legendre basis without the exponential weight does not provide satisfactory solutions to the inverse problem.

Boundary conditions for f_m . Recall from (1.5) that the time-dependent boundary observations are

$$\phi_0(t) = f(0, t), \quad \phi_L(t) = f(L, t), \quad \psi_0(t) = \partial_v f(0, t), \quad \psi_L(t) = \partial_v f(L, t), \quad t \in [0, T].$$

For each $m = 0, \dots, N$, define the corresponding Legendre–exponential coefficients

$$\begin{aligned} \phi_{0,m} &:= \int_0^T e^{-2t} \phi_0(t) \Psi_m(t) dt, & \phi_{L,m} &:= \int_0^T e^{-2t} \phi_L(t) \Psi_m(t) dt, \\ \psi_{0,m} &:= \int_0^T e^{-2t} \psi_0(t) \Psi_m(t) dt, & \psi_{L,m} &:= \int_0^T e^{-2t} \psi_L(t) \Psi_m(t) dt. \end{aligned}$$

Then the coefficient functions $\{f_m\}_{m=0}^N$ satisfy

$$f_m(0) = \phi_{0,m}, \quad f_m(L) = \phi_{L,m}, \quad f'_m(0) = \psi_{0,m}, \quad f'_m(L) = \psi_{L,m}, \quad m = 0, \dots, N. \quad (3.7)$$

In particular, since $f(0, t) = 0$ in (1.1), we have $\phi_{0,m} = 0$ and thus $f_m(0) = 0$ for all $m = 0, \dots, N$.

The reduced system. Combining (3.6) and (3.7), we obtain a coupled system of ODEs for

$$\mathbf{f}^N(v) = [f_0(v) \quad f_1(v) \quad \cdots \quad f_N(v)]^\top,$$

namely, for each $m = 0, 1, \dots, N$,

$$\begin{cases} -f''_m(v) + b(v)f'_m(v) + \sum_{n=0}^N s_{mn} f_n(v) = Q_m(\mathbf{f}^N)(v), & v \in (0, L), \\ f_m(0) = 0, \quad f_m(L) = \phi_{L,m}, \quad f'_m(0) = \psi_{0,m}, \quad f'_m(L) = \psi_{L,m}. \end{cases} \quad (3.8)$$

Remark 8 (Extension beyond the computational domain). *After restricting (3.8) to $v \in (0, L)$, the right-hand side still involves integrals over $(0, \infty)$ through the fragmentation gain term in Q_{frag} , namely*

$$2 \int_0^\infty V(v, v^*) f(v + v^*, t) dv^*,$$

which requires values of $f(\cdot, t)$ (and hence the modes $\{f_n\}_{n=0}^N$) at sizes $v + v^ > L$ even when $v \in (0, L)$. Therefore, to make $Q_m(\mathbf{f}^N)(v)$ well defined on $(0, L)$, one must prescribe an extension of the coefficient functions $\{f_n\}_{n=0}^N$ from $(0, L)$ to $(0, \infty)$.*

In this work, we adopt a continuous exponential tail extension: for each $n = 0, \dots, N$, we set

$$f_n(v) := f_n(L) e^{-(v-L)}, \quad v > L.$$

All occurrences of $Q_m(\mathbf{f}^N)(v)$ in (3.8) are understood with this extension when evaluating the fragmentation and coagulation operators.

Remark 9. *Let us note that, in order to solve the classical Boltzmann equation numerically, one also imposes a domain truncation (see [21, 23]). However, instead of using a continuous tail extension as above, the solution is assumed to be periodic on the truncated domain.*

Remark 10. *Equation (3.8) constitutes the **time-dimensional reduction model**. Solving (3.8) is the main step toward addressing Problem 1, since it yields $\mathbf{f}^N(v) = (f_0(v), \dots, f_N(v))^\top$. Once \mathbf{f}^N is obtained, the solution $f(v, t)$ can be reconstructed via the truncated expansion (3.1), i.e.,*

$$f(v, t) \approx \sum_{n=0}^N f_n(v) \Psi_n(t), \quad (v, t) \in (0, L) \times (0, T).$$

Consequently, the initial density is recovered by evaluating the reconstructed solution at $t = 0$,

$$f^0(v) = f(v, 0) \approx \sum_{n=0}^N f_n(v) \Psi_n(0), \quad v \in [0, L].$$

Solving (3.8) is nontrivial due to the nonlinear term $Q_m(\mathbf{f}^N)(v)$ and the intricate coagulation–fragmentation structure of the operator Q ; see (1.2)–(1.4) and Definition 1. To control this nonlinearity in the analysis below, we work under the following admissibility condition.

4 The Carleman–Picard iteration

As discussed in Remark 10, computing the solution of (3.8) is the central step in addressing Problem 1. A natural baseline strategy is to recover \mathbf{f}^* by solving (3.8) in a least-squares sense, i.e., by minimizing the nonlinear functional

$$J_{\text{ncvx}}(\varphi) := \sum_{m=0}^N \left[\int_0^L \left| -\varphi_m''(v) + b(v)\varphi_m'(v) + \sum_{n=0}^N s_{mn}\varphi_n(v) - Q_m(\varphi)(v) \right|^2 dv + |\varphi_m(0)|^2 + |\varphi_m(L) - \phi_{L,m}|^2 + |\varphi_m'(0) - \psi_{0,m}|^2 + |\varphi_m'(L) - \psi_{L,m}|^2 + \epsilon \|\varphi_m\|_{H^3(0,L)}^2 \right], \quad \varphi \in B. \quad (4.1)$$

Here, the admissible set B is introduced in Definition 2, and $\epsilon > 0$ is a small regularization parameter. This formulation is appealing and, in principle, robust, and therefore widely used in the mathematical and engineering communities. However, because $\mathbf{Q} = [Q_0 \ \dots \ Q_N]^\top$ has a complicated coagulation–fragmentation structure, the functional J_{ncvx} is generally nonconvex and may possess multiple local minimizers. Consequently, a direct minimization of (4.1) may fail to recover \mathbf{f}^* unless a sufficiently accurate initial guess is available.

To overcome this difficulty, we combine a Picard-type linearization with a Carleman-weighted least-squares minimization. The resulting Carleman–Picard scheme exploits the one-dimensional Carleman estimate in Lemma 1 to enforce stability and to guarantee convergence to \mathbf{f}^* .

Carleman–Picard update. Let

$$\mathbf{f}^{N,(0)}(v) = \begin{bmatrix} f_0^{(0)}(v) & f_1^{(0)}(v) & \cdots & f_N^{(0)}(v) \end{bmatrix}^\top \in B$$

be an initial guess, not necessarily close to the exact solution \mathbf{f}^* . Assume that, for some $k \geq 0$, the iterate

$$\mathbf{f}^{N,(k)}(v) = \begin{bmatrix} f_0^{(k)}(v) & f_1^{(k)}(v) & \cdots & f_N^{(k)}(v) \end{bmatrix}^\top \in B$$

is known. The next iterate $\mathbf{f}^{N,(k+1)}$ is defined as the unique minimizer of the Carleman-weighted functional

$$\mathbf{f}^{N,(k+1)} = \arg \min_{\boldsymbol{\varphi} \in B} J_{\lambda,\epsilon}^{\mathbf{f}^{N,(k)}}(\boldsymbol{\varphi}), \quad (4.2)$$

where $J_{\lambda,\epsilon}^{\mathbf{f}^{N,(k)}}$ is given by

$$\begin{aligned} J_{\lambda,\epsilon}^{\mathbf{f}^{N,(k)}}(\boldsymbol{\varphi}) = & \sum_{m=0}^N \left[\int_0^L e^{2\lambda r(v)^{-\beta}} \left| -\varphi_m''(v) + b(v)\varphi_m'(v) + \sum_{n=0}^N s_{mn} \varphi_n(v) - Q_m(\mathbf{f}^{N,(k)})(v) \right|^2 dv \right. \\ & + \lambda^4 e^{2\lambda r(0)^{-\beta}} |\varphi_m(0)|^2 + \lambda^4 e^{2\lambda r(L)^{-\beta}} |\varphi_m(L) - \phi_{L,m}|^2 + \lambda^4 e^{2\lambda r(0)^{-\beta}} |\varphi_m'(0) - \psi_{0,m}|^2 \\ & \left. + \lambda^4 e^{2\lambda r(L)^{-\beta}} |\varphi_m'(L) - \psi_{L,m}|^2 + \epsilon \|\varphi_m\|_{H^3(0,L)}^2 \right]. \quad (4.3) \end{aligned}$$

Here $\epsilon > 0$ is a regularization parameter, and the Carleman weight $e^{2\lambda r(v)^{-\beta}}$ is chosen as in Subsection 2.1. Recall that, in the evaluation of $J_{\lambda,\epsilon}^{\mathbf{f}^{N,(k)}}$, the vector $\mathbf{f}^{N,(k)}$ is extended to $v > L$ as described in Remark 8.

Remark 11 (Well-posedness of the minimization step). *Fix $k \geq 0$. Since the nonlinear term in (4.3) is evaluated at the known iterate $\mathbf{f}^{N,(k)}$, the functional $\boldsymbol{\varphi} \mapsto J_{\lambda,\epsilon}^{\mathbf{f}^{N,(k)}}(\boldsymbol{\varphi})$ is a quadratic functional of $\boldsymbol{\varphi}$. Moreover, the $H^3(0,L)$ -regularization term with $\epsilon > 0$ makes $J_{\lambda,\epsilon}^{\mathbf{f}^{N,(k)}}$ coercive and strictly convex on $[H^3(0,L)]^{N+1}$. Since $B \subset [H^3(0,L)]^{N+1}$ is closed and convex, the minimization problem (4.2) admits a unique minimizer in B .*

The theorem below guarantees the convergence of the Carleman–Picard method for solving (3.8).

Theorem 1. *Assume Assumption 1. Fix $\beta > 0$, and let λ_0 be as in Lemma 1. Let $\mathbf{f}^{N,(0)} \in B$, and for each $k \geq 0$, define $\mathbf{f}^{N,(k+1)}$ by (4.2). Let $\mathbf{f}^* \in B$ be the exact solution to (3.8). Then there exist $\lambda_1 \geq \lambda_0$ and a constant $C > 0$ such that, for all $\lambda \geq \lambda_1$ and all $\epsilon > 0$,*

$$\begin{aligned} & \int_0^L e^{2\lambda r(v)^{-\beta}} |\mathbf{f}^{N,(k+1)}(v) - \mathbf{f}^*(v)|^2 dv + e^{2\lambda r(L)^{-\beta}} |\mathbf{f}^{N,(k+1)}(L) - \mathbf{f}^*(L)|^2 \\ & \leq \frac{C}{\lambda^3} \left[\int_0^L e^{2\lambda r(v)^{-\beta}} |\mathbf{f}^{N,(k)}(v) - \mathbf{f}^*(v)|^2 dv + e^{2\lambda r(L)^{-\beta}} |\mathbf{f}^{N,(k)}(L) - \mathbf{f}^*(L)|^2 \right. \\ & \quad \left. + \epsilon \|\mathbf{f}^*\|_{[H^3(0,L)]^{N+1}}^2 \right]. \quad (4.4) \end{aligned}$$

Here, $C > 0$ depends only on L , β , v_0 , $\|b\|_{L^\infty(0,L)}$, N , $\{s_{mn}\}_{m,n=0}^N$, M , T , $\{\Psi_n\}_{n=0}^N$, K , and V , and is independent of k , λ , and ϵ .

In particular, let $\rho := \frac{C}{\lambda^3}$. If λ is sufficiently large so that $\rho \in (0, 1)$, then

$$\|\mathbf{f}^{N,(k)} - \mathbf{f}^*\|_\lambda^2 \leq \rho^k \|\mathbf{f}^{N,(0)} - \mathbf{f}^*\|_\lambda^2 + \frac{\rho\epsilon}{1-\rho} \|\mathbf{f}^*\|_{[H^3(0,L)]^{N+1}}^2, \quad k \geq 0, \quad (4.5)$$

where

$$\|\mathbf{g}\|_\lambda^2 := \int_0^L e^{2\lambda r(v)^{-\beta}} |\mathbf{g}(v)|^2 dv + e^{2\lambda r(L)^{-\beta}} |\mathbf{g}(L)|^2.$$

Consequently, $\{\mathbf{f}^{N,(k)}\}_{k \geq 0}$ converges geometrically to an ϵ -neighborhood of \mathbf{f}^* in the weighted norm $\|\cdot\|_\lambda$, and

$$\limsup_{k \rightarrow \infty} \|\mathbf{f}^{N,(k)} - \mathbf{f}^*\|_\lambda^2 \leq \frac{\rho\epsilon}{1-\rho} \|\mathbf{f}^*\|_{[H^3(0,L)]^{N+1}}^2.$$

Proof. Since B is convex and $\mathbf{f}^{N,(k+1)}$ minimizes $J_{\lambda,\epsilon}^{\mathbf{f}^{N,(k)}}$ over B , the standard variational inequality yields

$$DJ_{\lambda,\epsilon}^{\mathbf{f}^{N,(k)}}(\mathbf{f}^{N,(k+1)}) \left[\mathbf{y} - \mathbf{f}^{N,(k+1)} \right] \geq 0 \quad \text{for all } \mathbf{y} \in B.$$

In particular, since $\mathbf{f}^* \in B$, choosing $\mathbf{y} = \mathbf{f}^*$ gives

$$DJ_{\lambda,\epsilon}^{\mathbf{f}^{N,(k)}}(\mathbf{f}^{N,(k+1)}) \left[\mathbf{f}^* - \mathbf{f}^{N,(k+1)} \right] \geq 0. \quad (4.6)$$

Let

$$\mathbf{h} := \mathbf{f}^{N,(k+1)} - \mathbf{f}^*, \quad h_m := f_m^{(k+1)} - f_m^*, \quad m = 0, \dots, N. \quad (4.7)$$

Then $\mathbf{f}^* - \mathbf{f}^{N,(k+1)} = -\mathbf{h}$. By the linearity of the directional derivative in its direction argument, (4.6) is equivalent to

$$DJ_{\lambda,\epsilon}^{\mathbf{f}^{N,(k)}}(\mathbf{f}^{N,(k+1)}) \left[\mathbf{h} \right] \leq 0.$$

Using the definition (4.3) of $J_{\lambda,\epsilon}^{\mathbf{f}^{N,(k)}}$, we observe that the term $Q_m(\mathbf{f}^{N,(k)})(v)$ is evaluated at the known iterate $\mathbf{f}^{N,(k)}$ and is thus independent of $\boldsymbol{\varphi}$ in the differentiation with respect to $\boldsymbol{\varphi}$. Consequently, we obtain

$$\begin{aligned} DJ_{\lambda,\epsilon}^{\mathbf{f}^{N,(k)}}(\mathbf{f}^{N,(k+1)}) \left[\mathbf{h} \right] &= 2 \sum_{m=0}^N \left[\left\langle e^{2\lambda r(v)^{-\beta}} \left(-f_m^{(k+1)''}(v) + b(v)f_m^{(k+1)'}(v) + \sum_{n=0}^N s_{mn}f_n^{(k+1)}(v) \right. \right. \right. \\ &\quad \left. \left. - Q_m(\mathbf{f}^{N,(k)})(v) \right), -h_m''(v) + b(v)h_m'(v) + \sum_{n=0}^N s_{mn}h_n(v) \right\rangle_{L^2(0,L)} \\ &\quad + \lambda^4 e^{2\lambda r(0)^{-\beta}} (f_m^{(k+1)}(0))h_m(0) + \lambda^4 e^{2\lambda r(L)^{-\beta}} (f_m^{(k+1)}(L) - \phi_{L,m})h_m(L) \\ &\quad + \lambda^4 e^{2\lambda r(0)^{-\beta}} (f_m^{(k+1)'}(0) - \psi_{0,m})h_m'(0) + \lambda^4 e^{2\lambda r(L)^{-\beta}} (f_m^{(k+1)'}(L) - \psi_{L,m})h_m'(L) \\ &\quad \left. + \epsilon \left\langle f_m^{(k+1)}, h_m \right\rangle_{H^3(0,L)} \right] \leq 0. \quad (4.8) \end{aligned}$$

Since \mathbf{f}^* solves (3.8), we have, for each $m = 0, \dots, N$ and $v \in (0, L)$,

$$-f_m^{*''}(v) + b(v)f_m^{*'}(v) + \sum_{n=0}^N s_{mn}f_n^*(v) - Q_m(\mathbf{f}^*)(v) = 0,$$

and \mathbf{f}^* satisfies the boundary data in (3.8). Therefore,

$$\begin{aligned} 2 \sum_{m=0}^N \left[\left\langle e^{2\lambda r(v)^{-\beta}} \left(-f_m^{*''}(v) + b(v)f_m^{*'}(v) + \sum_{n=0}^N s_{mn}f_n^*(v) - Q_m(\mathbf{f}^*)(v) \right), \right. \right. \\ \left. \left. -h_m''(v) + b(v)h_m'(v) + \sum_{n=0}^N s_{mn}h_n(v) \right\rangle_{L^2(0,L)} + \lambda^4 e^{2\lambda r(0)^{-\beta}} f_m^*(0)h_m(0) \right. \\ \left. + \lambda^4 e^{2\lambda r(L)^{-\beta}} (f_m^*(L) - \phi_{L,m})h_m(L) + \lambda^4 e^{2\lambda r(0)^{-\beta}} (f_m^{*'}(0) - \psi_{0,m})h_m'(0) \right. \\ \left. + \lambda^4 e^{2\lambda r(L)^{-\beta}} (f_m^{*'}(L) - \psi_{L,m})h_m'(L) + \epsilon \left\langle f_m^*, h_m \right\rangle_{H^3(0,L)} \right] = 2\epsilon \sum_{m=0}^N \left\langle f_m^*, h_m \right\rangle_{H^3(0,L)}. \quad (4.9) \end{aligned}$$

Define, for $m = 0, \dots, N$,

$$\Delta_m^{(k)}(v) := Q_m(\mathbf{f}^*)(v) - Q_m(\mathbf{f}^{N,(k)})(v), \quad v \in (0, L).$$

Subtracting (4.9) from (4.8), using $\mathbf{f}^{N,(k+1)} = \mathbf{f}^* + \mathbf{h}$, and applying Young's inequality $XY \leq \frac{1}{2}X^2 + \frac{1}{2}Y^2$, we obtain

$$\begin{aligned} & \sum_{m=0}^N \left[\int_0^L e^{2\lambda r(v)^{-\beta}} \left| -h_m''(v) + b(v)h_m'(v) + \sum_{n=0}^N s_{mn}h_n(v) \right|^2 dv \right. \\ & \quad \left. + \lambda^4 e^{2\lambda r(0)^{-\beta}} (|h_m(0)|^2 + |h_m'(0)|^2) + \lambda^4 e^{2\lambda r(L)^{-\beta}} (|h_m(L)|^2 + |h_m'(L)|^2) + \epsilon \|h_m\|_{H^3(0,L)}^2 \right] \\ & \leq C \sum_{m=0}^N \int_0^L e^{2\lambda r(v)^{-\beta}} |\Delta_m^{(k)}(v)|^2 dv - 2\epsilon \sum_{m=0}^N \langle f_m^*, h_m \rangle_{H^3(0,L)} \end{aligned} \quad (4.10)$$

for some constant $C > 0$. As above, C denotes a generic constant depending only on $L, \beta, v_0, \|b\|_{L^\infty(0,L)}, N, \{s_{mn}\}_{m,n=0}^N, M, T, \{\Psi_n\}_{n=0}^N, K$, and V , and independent of k, λ , and ϵ . We do not keep track of the value of C .

Applying Lemma 4 and using (4.10), we have

$$\begin{aligned} & \sum_{m=0}^N \left[\int_0^L e^{2\lambda r(v)^{-\beta}} \left| -h_m''(v) + b(v)h_m'(v) + \sum_{n=0}^N s_{mn}h_n(v) \right|^2 dv \right. \\ & \quad \left. + \lambda^4 e^{2\lambda r(0)^{-\beta}} (|h_m(0)|^2 + |h_m'(0)|^2) + \lambda^4 e^{2\lambda r(L)^{-\beta}} (|h_m(L)|^2 + |h_m'(L)|^2) + \epsilon \|h_m\|_{H^3(0,L)}^2 \right] \\ & \leq C \int_0^L e^{2\lambda r(v)^{-\beta}} |\mathbf{f}^{N,(k)}(v) - \mathbf{f}^*(v)|^2 dv + C e^{2\lambda r(L)^{-\beta}} |\mathbf{f}^{N,(k)}(L) - \mathbf{f}^*(L)|^2 \\ & \quad + \epsilon \|\mathbf{f}^*\|_{[H^3(0,L)]^{N+1}}^2 + \epsilon \|\mathbf{h}\|_{[H^3(0,L)]^{N+1}}^2 \end{aligned} \quad (4.11)$$

Since $b \in L^\infty(0, \infty)$, applying the inequality

$$(X + Y + Z)^2 \geq \frac{1}{3}X^2 - Y^2 - Z^2$$

to the left-hand side of (4.11), we obtain

$$\begin{aligned} & \int_0^L e^{2\lambda r(v)^{-\beta}} |\mathbf{h}''(v)|^2 dv - C \int_0^L e^{2\lambda r(v)^{-\beta}} |\mathbf{h}'(v)|^2 dv - C \int_0^L e^{2\lambda r(v)^{-\beta}} |\mathbf{h}(v)|^2 dv \\ & \quad + \lambda^4 e^{2\lambda r(0)^{-\beta}} (|\mathbf{h}(0)|^2 + |\mathbf{h}'(0)|^2) + \lambda^4 e^{2\lambda r(L)^{-\beta}} (|\mathbf{h}(L)|^2 + |\mathbf{h}'(L)|^2) \\ & \leq C \int_0^L e^{2\lambda r(v)^{-\beta}} |\mathbf{f}^{N,(k)}(v) - \mathbf{f}^*(v)|^2 dv + C e^{2\lambda r(L)^{-\beta}} |\mathbf{f}^{N,(k)}(L) - \mathbf{f}^*(L)|^2 + \epsilon \|\mathbf{f}^*\|_{[H^3(0,L)]^{N+1}}^2. \end{aligned}$$

Applying Corollary 1 componentwise to h_m , summing over $m = 0, \dots, N$, and choosing λ sufficiently large, we obtain

$$\begin{aligned} & \int_0^L e^{2\lambda r(v)^{-\beta}} \left(\lambda^3 |\mathbf{h}(v)|^2 + \lambda |\mathbf{h}'(v)|^2 \right) dv \\ & \quad + \lambda^4 e^{2\lambda r(0)^{-\beta}} (|\mathbf{h}(0)|^2 + |\mathbf{h}'(0)|^2) + \lambda^4 e^{2\lambda r(L)^{-\beta}} (|\mathbf{h}(L)|^2 + |\mathbf{h}'(L)|^2) \\ & \leq C \int_0^L e^{2\lambda r(v)^{-\beta}} |\mathbf{f}^{N,(k)}(v) - \mathbf{f}^*(v)|^2 dv + C e^{2\lambda r(L)^{-\beta}} |\mathbf{f}^{N,(k)}(L) - \mathbf{f}^*(L)|^2 \\ & \quad + \epsilon \|\mathbf{f}^*\|_{[H^3(0,L)]^{N+1}}^2. \end{aligned} \quad (4.12)$$

Dropping the nonnegative terms

$$\lambda \int_0^L e^{2\lambda r(v)^{-\beta}} |\mathbf{h}'(v)|^2 dv, \quad \lambda^4 e^{2\lambda r(0)^{-\beta}} \left(|\mathbf{h}(0)|^2 + |\mathbf{h}'(0)|^2 \right), \quad \lambda^4 e^{2\lambda r(L)^{-\beta}} |\mathbf{h}'(L)|^2,$$

from the left-hand side of (4.12), and recalling (4.7), we obtain (4.4).

Define

$$E_k := \|\mathbf{f}^{N,(k)} - \mathbf{f}^*\|_\lambda^2.$$

Then (4.4) can be written as

$$E_{k+1} \leq \rho E_k + \rho \epsilon \|\mathbf{f}^*\|_{[H^3(0,L)]^{N+1}}^2, \quad \rho := \frac{C}{\lambda^3}.$$

Assume $\rho \in (0, 1)$. Iterating the recurrence yields

$$E_k \leq \rho^k E_0 + \rho \epsilon \|\mathbf{f}^*\|_{[H^3(0,L)]^{N+1}}^2 \sum_{j=0}^{k-1} \rho^j = \rho^k E_0 + \frac{\rho \epsilon}{1-\rho} \|\mathbf{f}^*\|_{[H^3(0,L)]^{N+1}}^2,$$

which is (4.5). This proves geometric convergence to an ϵ -dependent neighborhood of \mathbf{f}^* . \square

Remark 12. *Theorem 1 and the estimate (4.5) shows that the Carleman–Picard iteration converges to an ϵ -neighborhood of the exact solution \mathbf{f}^* in the weighted norm $\|\cdot\|_\lambda$. In particular, when the regularization parameter ϵ is chosen sufficiently small, the limiting point of the iteration can be regarded as a good approximation of the true solution \mathbf{f}^* . Therefore, in practical computations, one may expect the reconstructed coefficient vector $\mathbf{f}^{N,(k)}$ for large k to provide an accurate approximation of \mathbf{f}^* , up to a small regularization error controlled by ϵ .*

Theorem 1 and Remark 12 motivate the Carleman–Picard reconstruction procedure for Problem 1, which is summarized in Algorithm 1.

Algorithm 1 Carleman–Picard reconstruction for Problem 1

- 1: Choose the truncation index N , the Carleman parameters λ and β , and the regularization parameter ϵ .
- 2: Compute the data coefficients $\phi_{L,m}$, $\psi_{0,m}$, and $\psi_{L,m}$ for $m = 0, \dots, N$ from (1.5).
- 3: Choose an initial guess $\mathbf{f}^{N,(0)}(v) = \left[f_0^{(0)}(v) \quad \dots \quad f_N^{(0)}(v) \right]^\top \in B$ and a maximum number of iterations $K_{\max} > 0$.
- 4: **for** $k = 0, 1, \dots, K_{\max} - 1$ **do**
- 5: Extend the Fourier modes: for each $n = 0, \dots, N$, set

$$f_n^{(k)}(v) := f_n^{(k)}(L)e^{-(v-L)}, \quad v > L.$$

- 6: Compute

$$\mathbf{f}^{N,(k+1)} = \arg \min_{\varphi \in B} J_{\lambda,\epsilon}^{\mathbf{f}^{N,(k)}}(\varphi),$$

where $J_{\lambda,\epsilon}^{\mathbf{f}^{N,(k)}}$ is defined in (4.3).

- 7: **end for**
- 8: Reconstruct the space–time density on $(0, L) \times (0, T)$ by

$$f^{\text{rec}}(v, t) := \sum_{n=0}^N f_n^{(K_{\max})}(v) \Psi_n(t).$$

- 9: Output the reconstructed initial density

$$f_{\text{in}}^{\text{rec}}(v) := f^{\text{rec}}(v, 0) = \sum_{n=0}^N f_n^{(K_{\max})}(v) \Psi_n(0), \quad v \in [0, L].$$

In the next section, we describe the numerical implementation of Algorithm 1 and present illustrative reconstruction examples.

5 Numerical Experiments for the Carleman–Picard Method

In this section, we present numerical experiments to illustrate the performance of the Carleman–Picard method for Problem 1. We first describe how synthetic boundary data are generated by numerically solving the forward coagulation–fragmentation equation. We then describe the numerical implementation of the reconstruction algorithm and present several tests on noisy data. The results demonstrate that the proposed method yields accurate and stable reconstructions for a variety of representative initial densities.

5.1 Generation of synthetic data by solving the forward problem

To generate synthetic boundary data for the inverse problem, we first solve the forward coagulation–fragmentation equation numerically. In all experiments, we take $b(v) \equiv 1$ and choose the coagulation and fragmentation kernels

$$K(v, v^*) = v + v^*, \quad V(v, v^*) = v + v^*.$$

The initial density f_{in} is selected from the family of test profiles described below.

Truncation of the half-line. The forward problem is posed for $v \in (0, \infty)$. In computations, we truncate the size domain to a finite interval $(0, R)$ with $R = 10$. This truncation is justified by the rapid decay of the size distribution for large v observed in our simulations; in particular, we enforce the homogeneous boundary condition

$$f(R, t) = 0, \quad t \in (0, T),$$

as a numerical surrogate for the decay condition $f(v, t) \rightarrow 0$ as $v \rightarrow \infty$.

Discretization. We solve the forward problem on $(0, R) \times (0, T)$ with $T = 0.5$. The size variable is discretized on a uniform grid with $N_v = 241$ nodes,

$$v_i = (i - 1)\Delta v, \quad i = 1, \dots, N_v,$$

with mesh size

$$\Delta v = \frac{R}{N_v - 1}.$$

Time is discretized on a uniform grid with $N_t = 301$ nodes,

$$t_n = (n - 1)\Delta t, \quad n = 1, \dots, N_t,$$

with a time step

$$\Delta t = \frac{T}{N_t - 1}.$$

Time stepping. To improve stability, we use a semi-implicit time-stepping method. Denoting by f_i^n the approximation of $f(v_i, t_n)$, we evaluate the collision operator explicitly at time level t_n , while the size-transport and size-diffusion terms are treated implicitly at time level t_{n+1} . More precisely, at each time step, we solve

$$\frac{f^{n+1} - f^n}{\Delta t} = -\partial_v f^{n+1} + \partial_{vv} f^{n+1} + Q(f^n),$$

where the derivatives in v are approximated by standard finite differences on the size grid. The resulting linear system at each time step is solved in the least-squares sense to accommodate the boundary constraints on $(0, R)$.

Discrete evaluation of the collision operator. The collision operator $Q = Q_{\text{coag}} + Q_{\text{frag}}$ is evaluated on the size grid by direct quadrature (discrete summation). Since the forward computation is performed on the truncated interval $(0, R)$ with the decay surrogate $f(R, t) = 0$, any term requiring values beyond R (e.g., $f(v + v^*, t)$ with $v + v^* > R$) is set to zero in the discrete implementation. This is consistent with the truncation of the half-line and with the imposed boundary condition at $v = R$.

Restriction to the inverse domain and noise. After computing the forward solution on the larger domain $(0, R) \times (0, T)$, we restrict it to the inverse domain

$$(0, L) \times (0, T), \quad L = 2,$$

by interpolation onto the reconstruction grid. We then define the exact boundary data

$$\phi_L^{\text{true}}(t) = f^{\text{true}}(L, t), \quad \psi_0^{\text{true}}(t) = \partial_v f^{\text{true}}(0, t), \quad \psi_L^{\text{true}}(t) = \partial_v f^{\text{true}}(L, t), \quad t \in (0, T).$$

Since the model imposes the boundary condition $f(0, t) = 0$, we have

$$\phi_0(t) = 0,$$

so this datum is kept exact and is not perturbed by noise.

To simulate measurement errors, we corrupt the remaining boundary observations by multiplicative noise:

$$\begin{aligned} \phi_L^\delta(t) &= \phi_L^{\text{true}}(t)(1 + \delta \xi_1(t)), \\ \psi_0^\delta(t) &= \psi_0^{\text{true}}(t)(1 + \delta \xi_2(t)), \\ \psi_L^\delta(t) &= \psi_L^{\text{true}}(t)(1 + \delta \xi_3(t)). \end{aligned}$$

for $t \in (0, T)$ where $\delta > 0$ is the noise level and ξ_1, ξ_2, ξ_3 are independent random functions uniformly distributed in $[-1, 1]$.

5.2 Numerical Implementation

In this subsection, we present some details of the implementation of Algorithm 1.

Step 1: Choice of N , λ , β , and ϵ .

The parameters are chosen empirically. We first select one numerical example, namely **Test 1** below, as the reference test.

The truncation index N is determined by comparing the forward solution $f(L, t)$ with its truncated Legendre–exponential expansion

$$\sum_{n=0}^N f_n(L) \Psi_n(t)$$

at the noise-free level (0% noise). More precisely, we introduce the function $\varphi : \mathbb{N} \rightarrow \mathbb{R}$, which measures the relative discrepancy between $f(L, t)$, ($t \in (0, T)$), and the truncation of its Fourier expansion with respect to the polynomial–exponential basis. It is defined by

$$\varphi(N) = \frac{\left\| f(L, t) - \sum_{n=0}^N f_n(L) \Psi_n(t) \right\|_{L^\infty(0, T)}}{\|f(L, t)\|_{L^\infty(0, T)}}. \quad (5.1)$$

It is interesting to observe from Figure 1a that the graph of φ has an L -curve shape. This observation somewhat confirms that N serves as a regularization factor. For Test 1, we choose $N = 20$, which corresponds to the corner of the L -curve. Numerically, we also observe that larger values of N , for example $25 \leq N \leq 45$, produce similar reconstruction results. Figure 1b shows that the truncated expansion with $N = 20$ matches the forward data $f(L, t)$ very well over the entire observation interval. The two graphs are almost indistinguishable, indicating that the first 20 basis functions already capture the essential temporal behavior of the signal. This observation supports the choice $N = 20$ as a suitable truncation level for the reconstruction procedure.

Once N is fixed, the remaining parameters λ , β , and ϵ are selected by trial and error so that the reconstruction quality for the reference test is satisfactory. After this calibration step, the same parameter values are used for all other numerical examples reported in this paper.

In all reconstruction experiments, we take the truncation number and regularization parameters to be

$$N = 20, \quad \beta = 10, \quad \lambda = 2, \quad \epsilon = 10^{-6.5}.$$

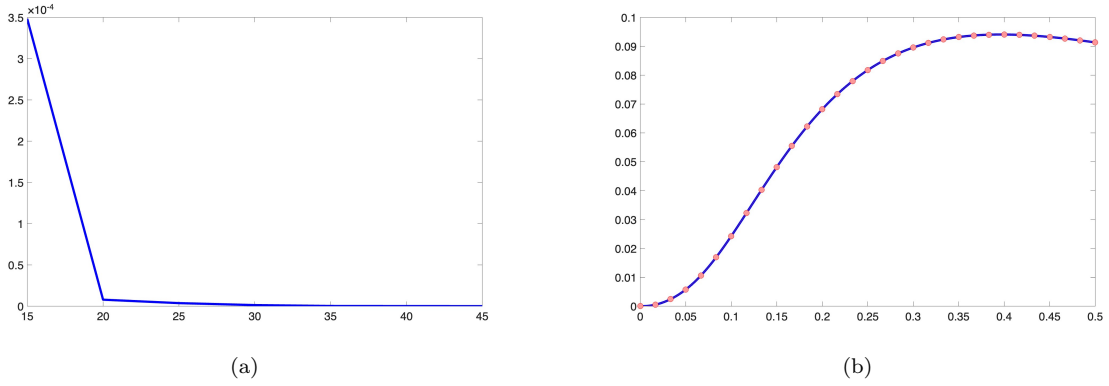


Figure 1: (a) The graph of the function $\varphi : \{15, \dots, 45\} \rightarrow \mathbb{R}$ defined in (5.1), computed from Test 1 below. (b) Comparison between the forward solution $f(L, t)$ and its truncated Legendre-exponential expansion with $N = 20$ over the interval $t \in [0, T]$. The blue curve represents $f(L, t)$, while the red markers denote its truncated expansion.

Step 3: Initial guess and maximum number of iterations. For the initialization, we choose the initial guess to be the zero function, that is,

$$\mathbf{f}^{N,(0)}(v) = 0 \quad \text{for all } v \in (0, L).$$

Equivalently, each initial mode is set to

$$f_n^{(0)}(v) = 0, \quad n = 0, \dots, N.$$

This choice provides a simple baseline initialization and is consistent with the convergence result established for the Carleman–Picard iteration. In all numerical experiments, the maximum number of iterations is fixed at $K_{\max} = 9$.

Step 6: Numerical realization of the minimization step. In the implementation, the update

$$\mathbf{f}^{N,(k+1)} = \arg \min_{\varphi \in B} J_{\lambda, \epsilon}^{\mathbf{f}^{N,(k)}}(\varphi)$$

is carried out at the discrete level as a regularized constrained least-squares problem.

More precisely, for a given iterate $\mathbf{f}^{N,(k)}$, we first evaluate the coagulation–fragmentation operator at $\mathbf{f}^{N,(k)}$ in the physical variables (v, t) . The resulting function is then projected onto the truncated Legendre–exponential basis in time and rewritten in vectorized form with respect to the spatial grid and the mode index. In this way, we obtain the discrete right-hand side associated with the frozen nonlinear terms

$$Q_m(\mathbf{f}^{N,(k)}), \quad m = 0, \dots, N.$$

Next, we assemble the discrete linear operator corresponding to the left-hand side of the reduced system

$$-f_m''(v) + b(v)f_m'(v) + \sum_{n=0}^N s_{mn}f_n(v), \quad m = 0, \dots, N,$$

together with the Tikhonov regularization term. After freezing the nonlinear operator at the previous iterate, Step 6 reduces to a linear constrained optimization problem. The new iterate $\mathbf{f}^{N,(k+1)}$ is then computed by solving the resulting regularized least-squares system subject to the boundary constraints at $v = 0$ and $v = L$. Therefore, the numerical implementation of Step 6 consists of three main substeps: evaluation of the frozen nonlinear source at $\mathbf{f}^{N,(k)}$, projection onto the truncated time basis, and solution of the corresponding regularized constrained linear least-squares problem for $\mathbf{f}^{N,(k+1)}$. The discrete minimization problem arising at each Carleman–Picard step is solved by the MATLAB constrained least-squares solver `lsqlin`.

The other steps in Algorithm 1 are implemented straightforwardly according to their definitions. In particular, the extension beyond $v = L$, the reconstruction of the space–time density, and the recovery of the initial profile are performed directly using the corresponding formulas in the algorithm.

5.3 Numerical reconstruction results

In this section, we display some numerical tests.

Test 1: For Test 1, we choose the true initial density to be

$$f^0(v) = \begin{cases} \frac{\pi}{2} \sin(\pi v), & 0 \leq v \leq 1, \\ 0, & v > 1. \end{cases}$$

The function is smooth on $(0, 1)$, vanishes at both $v = 0$ and $v = 1$, and has compact support in $[0, 1]$. Figure 2 displays the reconstruction results for Test 1 at the noise levels 5% and 10%.

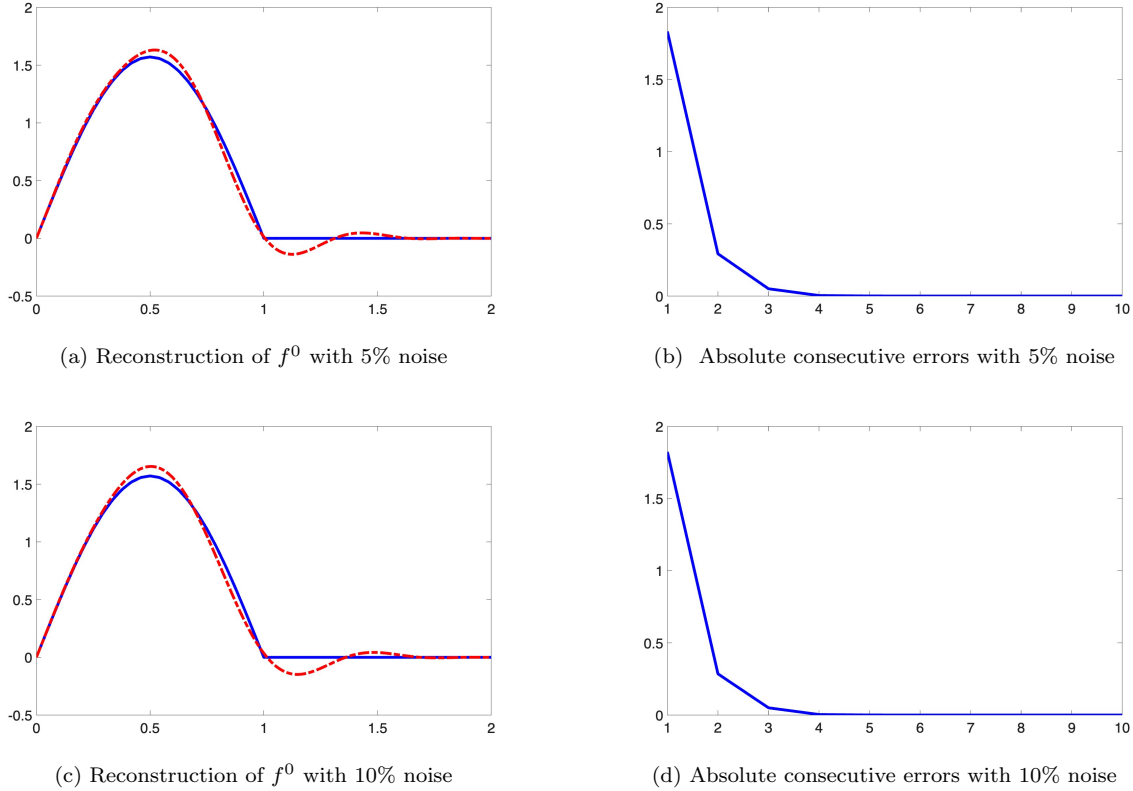


Figure 2: Test 1. The first row shows the results for the 5% noise level, while the second row shows the results for the 10% noise level. In each row, the left plot compares the true initial density and its reconstruction: the solid curve denotes the true function, and the dashed curve denotes the reconstructed one. The right plot shows the absolute consecutive error $\|f^{\text{rec},(k+1)} - f^{\text{rec},(k)}\|_{L^\infty(0,L)}$.

The results in Figure 2 show that the proposed method reconstructs the true initial density well for both noise levels. In particular, the reconstructed function matches the true one closely in shape and amplitude for $\delta = 5\%$, and it remains stable and accurate for $\delta = 10\%$. To quantify the reconstruction accuracy, we use the relative L^2 error $\frac{\|f^{0,\text{true}} - f^{0,\text{rec}}\|_{L^2(0,L)}}{\|f^{0,\text{true}}\|_{L^2(0,L)}}$ and the relative L^∞ error $\frac{\|f^{0,\text{true}} - f^{0,\text{rec}}\|_{L^\infty(0,L)}}{\|f^{0,\text{true}}\|_{L^\infty(0,L)}}$. For the 5% noise level, these errors are 0.0700 and 0.0880, respectively. For the 10% noise level, they are 0.0781 and 0.0942, respectively. These results indicate that the proposed method yields accurate reconstructions and remains robust in the presence of noise. Moreover, the absolute consecutive errors decrease rapidly over iterations, confirming the stable numerical behavior of the Carleman–Picard scheme.

Test 2: For Test 2, the true initial density is given by the probability density function of the Gaussian distribution

$$f^0(v) = \frac{1}{\sqrt{2\pi}\sigma} \exp\left(-\frac{(v - \mu)^2}{2\sigma^2}\right), \quad \mu = 0.7, \quad \sigma = 0.2.$$

The function is smooth and positive on $(0, L)$, with its peak located at $v = 0.7$. Figure 3 displays the reconstruction results for Test 1 at the noise levels 5% and 10%.

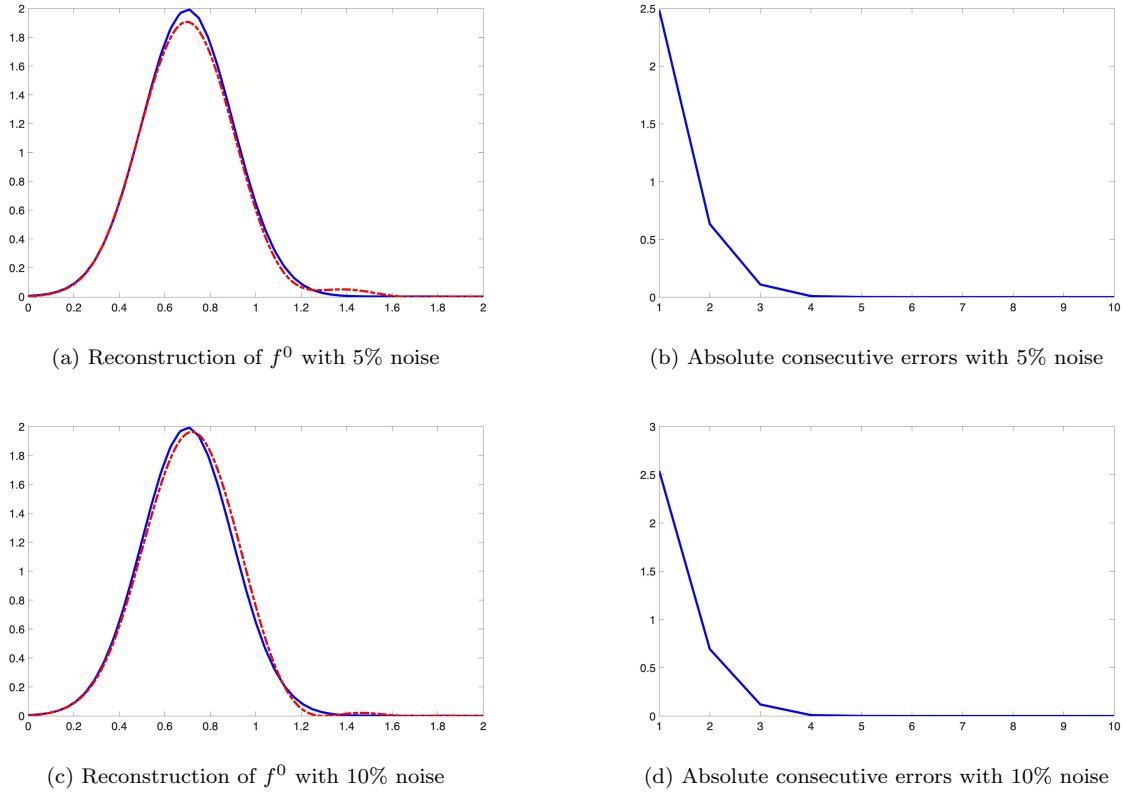


Figure 3: Test 2. The first row shows the results for the 5% noise level, while the second row shows the results for the 10% noise level. In each row, the left plot compares the true initial density and its reconstruction: the solid curve denotes the true function, and the dashed curve denotes the reconstructed one. The right plot shows the absolute consecutive error $\|f^{\text{rec},(k+1)} - f^{\text{rec},(k)}\|_{L^\infty(0,L)}$.

The reconstructions shown in Figure 3 demonstrate that the proposed method performs well for this smooth Gaussian initial density. For both noise levels, the reconstructed function accurately captures the location, width, and overall shape of the true initial density. To quantify the reconstruction accuracy, we use the relative L^2 error $\frac{\|f^{0,\text{true}} - f^{0,\text{rec}}\|_{L^2(0,L)}}{\|f^{0,\text{true}}\|_{L^2(0,L)}}$ and the relative L^∞ error $\frac{\|f^{0,\text{true}} - f^{0,\text{rec}}\|_{L^\infty(0,L)}}{\|f^{0,\text{true}}\|_{L^\infty(0,L)}}$. For the 5% noise level, these errors are 0.0420 and 0.0441, respectively. For the 10% noise level, they are 0.0612 and 0.0728, respectively. These results indicate that the proposed method yields accurate reconstructions and maintains good robustness under noisy data. Moreover, the absolute consecutive errors decrease rapidly over iterations, confirming the stable numerical behavior of the Carleman–Picard scheme.

Test 3: In Test 3, the true initial density is chosen as the probability density function of the uniform distribution

$$f^0(v) = \begin{cases} 2.5, & 0.6 \leq v \leq 1, \\ 0, & \text{otherwise.} \end{cases}$$

This function is compactly supported on $[0.6, 1]$ and has jump discontinuities at $v = 0.6$ and $v = 1$, where it changes abruptly between 0 and 2.5. Therefore, this example is more challenging than the previous two tests, since the target function is discontinuous.

The reconstructions in Figure 4 show that the proposed method remains effective even for this discontinuous initial density. Although the relative L^2 and L^∞ errors are larger than those in the previous smooth

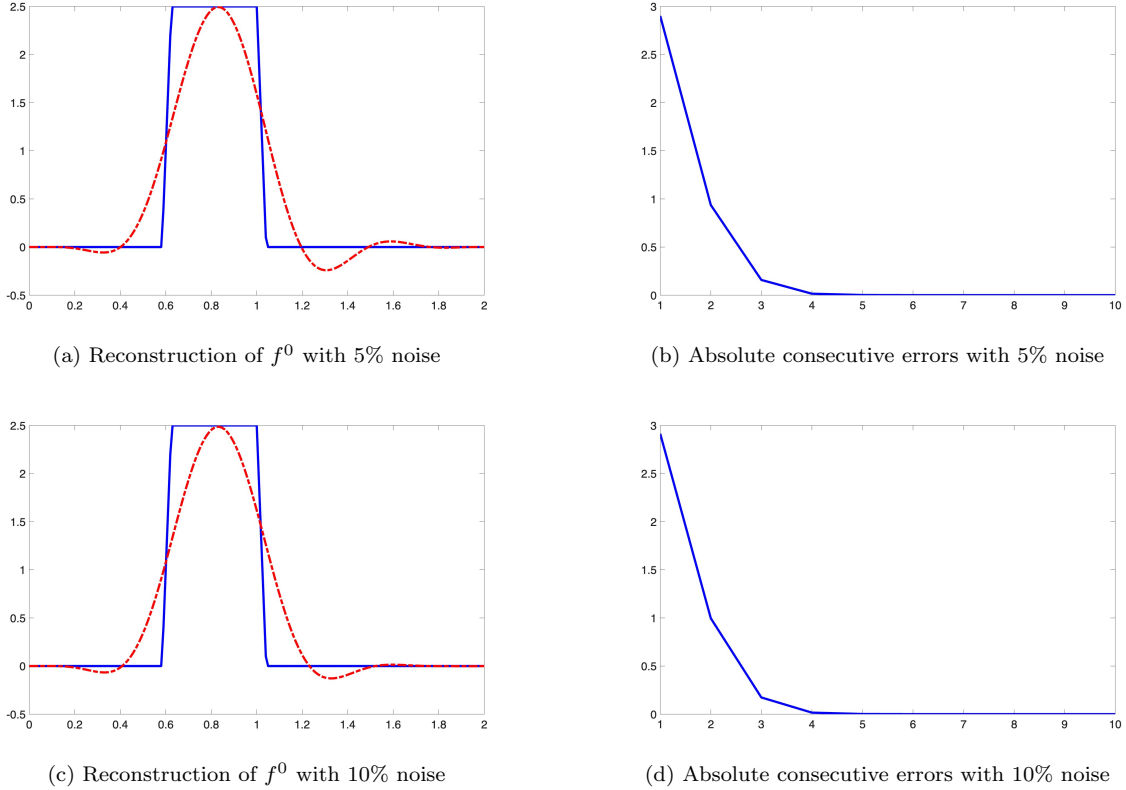


Figure 4: Test 3. The first row shows the results for the 5% noise level, while the second row shows the results for the 10% noise level. In each row, the left plot compares the true initial density and its reconstruction: the solid curve denotes the true function, and the dashed curve denotes the reconstructed one. The right plot shows the absolute consecutive error $\|f^{\text{rec},(k+1)} - f^{\text{rec},(k)}\|_{L^\infty(0,L)}$.

tests, the reconstructed function still captures the main qualitative features of the true initial density, including the location of its support, the approximate height of the plateau, and the overall block-type structure. This behavior is reasonable because the true solution exhibits jump discontinuities, whereas the reconstruction procedure is based on a regularized least-squares formulation and therefore tends to produce smoother approximations near discontinuities. As a result, some smearing and oscillation near the jump locations are expected.

To quantify the reconstruction accuracy, we use the relative L^2 error $\frac{\|f^{0,\text{true}} - f^{0,\text{rec}}\|_{L^2(0,L)}}{\|f^{0,\text{true}}\|_{L^2(0,L)}}$ and the relative L^∞ error $\frac{\|f^{0,\text{true}} - f^{0,\text{rec}}\|_{L^\infty(0,L)}}{\|f^{0,\text{true}}\|_{L^\infty(0,L)}}$. For the 5% noise level, these errors are 0.3106 and 0.4631, respectively. For the 10% noise level, they are 0.3154 and 0.4692, respectively. The fact that these values change only slightly when the noise level increases from 5% to 10% indicates a certain degree of robustness of the method with respect to noise, even in this more challenging nonsmooth setting. Moreover, the absolute consecutive errors decrease rapidly over iterations, confirming the stable numerical behavior of the Carleman–Picard scheme.

Test 4: In Test 4, the true initial density is chosen as the probability density function of a scaled Beta distribution:

$$f^0(v) = \begin{cases} \frac{1}{2B(3,7)} \left(\frac{v}{2}\right)^2 \left(1 - \frac{v}{2}\right)^6, & 0 \leq v \leq 2, \\ 0, & v > 2, \end{cases}$$

where $B(3, 7)$ denotes the Beta function evaluated at $(3, 7)$, that is,

$$B(3, 7) = \int_0^1 t^2(1-t)^6 dt.$$

This function is nonnegative and smooth on $(0, 2)$, and it vanishes at both endpoints $v = 0$ and $v = 2$.

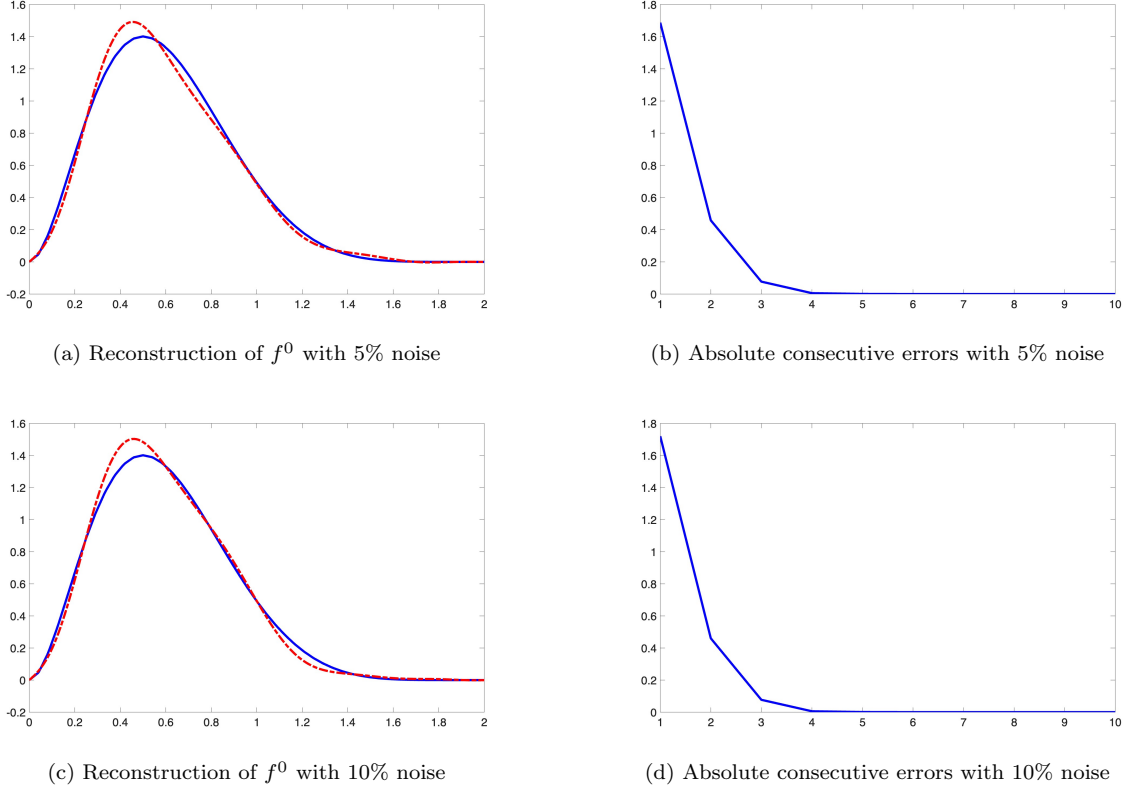


Figure 5: Test 4. The first row shows the results for the 5% noise level, while the second row shows the results for the 10% noise level. In each row, the left plot compares the true initial density and its reconstruction: the solid curve denotes the true function, and the dashed curve denotes the reconstructed one. The right plot shows the absolute consecutive error $\|f^{\text{rec},(k+1)} - f^{\text{rec},(k)}\|_{L^\infty(0,L)}$.

The reconstructions in Figure 5 show that the proposed method performs well for this scaled Beta-type initial density. For both noise levels, the reconstructed function accurately reproduces the main characteristics of the true initial density, including the peak location, the overall asymmetric shape, and the decay toward both endpoints. To quantify the reconstruction accuracy, we use the relative L^2 error $\frac{\|f^{0,\text{true}} - f^{0,\text{rec}}\|_{L^2(0,L)}}{\|f^{0,\text{true}}\|_{L^2(0,L)}}$ and the relative L^∞ error $\frac{\|f^{0,\text{true}} - f^{0,\text{rec}}\|_{L^\infty(0,L)}}{\|f^{0,\text{true}}\|_{L^\infty(0,L)}}$. For the 5% noise level, these errors are 0.0657 and 0.0930, respectively. For the 10% noise level, they are 0.0649 and 0.0982, respectively. These values indicate that the proposed method yields accurate reconstructions and remains stable under noisy data. Moreover, the absolute consecutive errors decrease rapidly over iterations, confirming the stable numerical behavior of the Carleman–Picard scheme.

Remark 13. *The numerical results provide clear evidence of the fast convergence of the Carleman–Picard iteration. In particular, the consecutive errors decrease rapidly as the iteration number increases; see, for example, Figures 2b and 2d. This decay is consistent with the geometric rate ρ^k predicted by Theorem 1, where $\rho \in (0, 1)$. Hence, the numerical experiments confirm the global convergence analysis and show that the proposed method converges rapidly in practical computations.*

Remark 14. Although the objective of the inverse problem is to recover the initial density $f(v, 0)$, our method actually yields an approximation of the full function $f(v, t)$ for all $(v, t) \in [0, L] \times [0, T]$. Indeed, once the coefficient functions are reconstructed, the function $f^{\text{rec}}(v, t)$ can be computed for every $(v, t) \in [0, L] \times [0, T]$ using the approximation formula in Step 8 of Algorithm 1. Therefore, the numerical algorithm recovers not only the initial profile but also the entire time-dependent solution on the reconstruction domain.

In this paper, however, we report mainly the profile $f(v, 0)$, since this is the unknown quantity of principal interest in the inverse problem. For illustration, in Figure 6, we include in Test 3 the reconstructed full field $f^{\text{rec}}(v, t)$, the corresponding exact solution $f^{\text{true}}(v, t)$, and the pointwise relative error, which is computed as

$$\mathcal{E}(v, t) = \frac{|f^{\text{true}} - f^{\text{rec}}|}{\|f^{\text{true}}\|_{L^\infty((0,L) \times (0,T))}},$$

on $[0, L] \times [0, T]$. These additional plots show that the computed solution agrees well with the true one over the entire space-time domain, with larger errors concentrated only in a few limited regions.

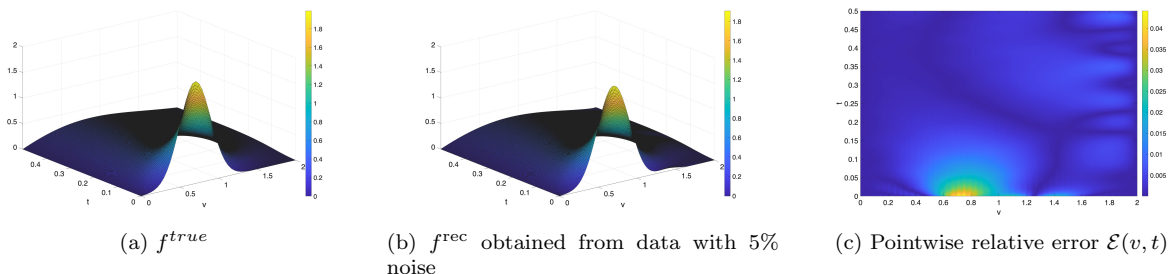


Figure 6: Test 3. Full space-time reconstruction on $[0, L] \times [0, T]$: (a) exact solution $f^{\text{true}}(v, t)$, (b) reconstructed solution $f^{\text{rec}}(v, t)$ from data with 5% noise, and (c) pointwise relative error $\mathcal{E}(v, t)$. The reconstructed surface is in good agreement with the true one over most of the domain.

6 Concluding remarks

In this paper, we investigated an inverse initial-density problem for a coagulation–fragmentation equation with size convection–diffusion. The objective was to reconstruct the unknown initial particle-size distribution from time-dependent boundary observations of the solution and its size derivative. To solve this problem, we developed a globally convergent reconstruction method that combines a Legendre–exponential time reduction with a Carleman–Picard iterative procedure.

The method first eliminates the time variable by projecting the solution onto a truncated polynomial–exponential basis, thereby reducing the original inverse problem to a coupled system for the spatial–mode coefficients. This reduced nonlinear system is then solved by a Carleman-weighted Picard iteration. The global convergence of the method is ensured by the Carleman weight and the associated Carleman estimate. At the same time, truncating the Fourier expansion improves stability by filtering out highly oscillatory noise components.

Under the assumptions imposed in this paper, we established a rigorous convergence result for the Carleman–Picard iteration and obtained a complete reconstruction procedure for the unknown initial density. The numerical experiments confirm the theoretical analysis and show that the proposed method yields accurate and stable reconstructions for several representative examples, including both smooth and nonsmooth initial profiles and noisy boundary data.

Acknowledgment

M.-B. Tran is funded in part by NSF CAREER DMS-2303146 and NSF Grants DMS-2305523 and DMS-2306379.

References

- [1] R. Abney, T. T. Le, L. H. Nguyen, and C. Peters. A Carleman-Picard approach for reconstructing zero-order coefficients in parabolic equations with limited data. *Applied Mathematics and Computation*, 494:129286, 2025.
- [2] V. I. Agoshkov and P. B. Dubovski. Solution of the reconstruction problem of a source function in the coagulation-fragmentation equation. *Russian Journal of Numerical Analysis and Mathematical Modelling*, 17(4):319–330, 2002.
- [3] V. I. Agoshkov and P. B. Dubovski. Solution of the reconstruction problem of a source function in the coagulation-fragmentation equation. *Russian Journal of Numerical Analysis and Mathematical Modelling*, 17(4):319–330, 2002.
- [4] O. Alomari and P.B. Dubovski. Recovery of the integral kernel in the kinetic fragmentation equation. *Inverse Problems in Science and Engineering*, 21(1):171–181, 2013.
- [5] D. Balagué, J. Cañizo, and P. Gabriel. Fine asymptotics of profiles and relaxation to equilibrium for growth-fragmentation equations with variable drift rates. *Kinetic and related models*, 6(2):219–243, 2013.
- [6] J. M. Ball and J. Carr. The discrete coagulation-fragmentation equations: Existence, uniqueness, and density conservation. *Journal of Statistical Physics*, 61(1-2):203–234, October 1990.
- [7] J. Banasiak and L. Arlotti. *Perturbations of Positive Semigroups with Applications*. Springer Monographs in Mathematics. Springer London, 2006.
- [8] J. Banasiak, W. Lamb, and P. Laurencot. *Analytic Methods for Coagulation-Fragmentation Models, I & II*. Chapman et Hall, 2019.
- [9] V. Bansaye, B. Cloez, P. Gabriel, and A. Marguet. A non-conservative harris ergodic theorem. *Journal of the London Mathematical Society*, 106(3):2459–2510, 2022.
- [10] J. Bertoin. Eternal solutions to Smoluchowski’s coagulation equation with additive kernel and their probabilistic interpretations. *The Annals of Applied Probability*, 12(2):547 – 564, 2002.
- [11] J. Bertoin. The asymptotic behavior of fragmentation processes. *Journal of the European Mathematical Society*, 005:395–416, 2003.
- [12] J. Bertoin. *Random Fragmentation and Coagulation Processes*, volume 102 of *Cambridge Studies in Advanced Mathematics*. Cambridge University Press, Cambridge, August 2006.
- [13] M. J. Cáceres, J. A. Cañizo, and S. Mischler. Rate of convergence to the remarkable state for the self-similar fragmentation and growth-fragmentation equations. *Journal de Mathématiques Pures et Appliquées*, 96(4):334–362, 2011.
- [14] J.A. Carrillo, R.M. Colombo, P. Gwiazda, and A. Ulikowska. Structured populations, cell growth and measure valued balance laws. *Journal of Differential Equations*, 252(4):3245–3277, 2012.
- [15] Trong D. Dang, Chanh V. Le, Khoa D. Luu, and Loc H. Nguyen. Recovery of initial displacement and velocity in anisotropic elastic systems by the time dimensional reduction method. *Journal of Computational Physics*, 542:114371, 2025.
- [16] A. Das and M.-B. Tran. Numerical schemes for a fully nonlinear coagulation–fragmentation model coming from wave kinetic theory. *Proceedings of the Royal Society A: Mathematical, Physical and Engineering Sciences*, 481(2316), 2025.
- [17] M. Doumic, M. Escobedo, and M. Tournus. Estimating the division rate and kernel in the fragmentation equation. *Ann. Inst. H. Poincaré Anal. Non Linéaire*, 35(7):1847–1884, 2018.

- [18] M. Doumic, M. Escobedo, and M. Tournus. An inverse problem: recovering the fragmentation kernel from the short-time behaviour of the fragmentation equation. *Annales Henri Lebesgue*, 7:621–671, 2024.
- [19] P. B. Dubovski and I. W. Stewart. Existence, uniqueness and mass conservation for the coagulation-fragmentation equation. *Mathematical Methods in The Applied Sciences*, 19:571–591, 1996.
- [20] F. Filbet and P. Laurençot. Numerical simulation of the smoluchowski coagulation equation. *SIAM Journal on Scientific Computing*, 25(6):2004–2028, 2004.
- [21] F. Filbet, C. Mouhot, and L. Pareschi. Solving the boltzmann equation in $n \log^2 n$. *SIAM Journal on Scientific Computing*, 28(3):1029–1053, 2006.
- [22] A. Friedman and F. Reitich. A hyperbolic inverse problem arising in the evolution of combustion aerosol. *Archive for Rational Mechanics and Analysis*, 110(4):313–350, 1990.
- [23] I. M. Gamba and S. H. Tharkabhushanam. Spectral-lagrangian methods for collisional models of non-equilibrium statistical states. *Journal of Computational Physics*, 228(6):2012–2036, 2009.
- [24] V. H. Hoang, T.M. Pham Ngoc, V. Rivoirard, and V.C. Tran. Nonparametric estimation of the fragmentation kernel based on a partial differential equation stationary distribution approximation. *Scandinavian Journal of Statistics*, 49(1):4–43, 2022.
- [25] J. Jang and H. V. Tran. Discrete coagulation-fragmentation equations with multiplicative coagulation kernel and constant fragmentation kernel. *Advances in Continuous and Discrete Models*, 2025(1):86, 2025.
- [26] P. P. Jones, Robin C. Ball, and Colm Connaughton. Nonlinear least-squares method for the inverse droplet coagulation problem. *Phys. Rev. E*, 88:012138, Jul 2013.
- [27] M. Kostoglou and A.J. Karabelas. On the self-similar solution of fragmentation equation: Numerical evaluation with implications for the inverse problem. *Journal of Colloid and Interface Science*, 284:571–581, 2005.
- [28] P. Laurençot and C. Walker. Well-posedness of the coagulation-fragmentation equation with size diffusion. *Differential and integral equations*, 35(3/4):211–240, 2022.
- [29] P. N. H. Le, T. T. Le, and L. H. Nguyen. The Carleman convexification method for Hamilton-Jacobi equations. *Computers and Mathematics with Applications*, 159:173–185, 2024.
- [30] T. T. Le. Global reconstruction of initial conditions of nonlinear parabolic equations via the Carleman-contraction method. In D-L. Nguyen, L. H. Nguyen, and T-P. Nguyen, editors, *Advances in Inverse problems for Partial Differential Equations*, volume 784 of *Contemporary Mathematics*, pages 23–42. American Mathematical Society, 2023.
- [31] T. T. Le, M. V. Klivanov, L. H. Nguyen, A. Sullivan, and L. Nguyen. Carleman contraction mapping for a 1D inverse scattering problem with experimental time-dependent data. *Inverse Problems*, 38:045002, 2022.
- [32] T. T. Le and L. H. Nguyen. A convergent numerical method to recover the initial condition of nonlinear parabolic equations from lateral Cauchy data. *Journal of Inverse and Ill-posed Problems*, 30(2):265–286, 2022.
- [33] T. T. Le, L. V. Nguyen, L. H. Nguyen, and H. Park. The time dimensional reduction method to determine the initial conditions without the knowledge of damping coefficients. *Computers and Mathematics with Applications*, 166:77–90, 2024.
- [34] B.-V. Matioc, L. Roberti, and C. Walker. Quasilinear parabolic equations with superlinear nonlinearities in critical spaces. *Journal of Differential Equations*, 429:283–317, 2025.

- [35] D. J. McLaughlin, W. Lamb, and A. C. McBride. An existence and uniqueness result for a coagulation and multiple-fragmentation equation. *SIAM Journal on Mathematical Analysis*, 28(5):1173–1190, 1997.
- [36] Z. A. Melzak. A scalar transport equation. *Trans. Amer. Math. Soc.*, 85:547–560, 1957.
- [37] G. Narsimhan, D. Ramkrishna, and J. P. Gupta. Analysis of drop size distributions in lean liquid-liquid dispersions. *AIChE Journal*, 26(6):991–1000, 1980.
- [38] L. H. Nguyen. The Carleman contraction mapping method for quasilinear elliptic equations with overdetermined boundary data. *Acta Mathematica Vietnamica*, 48:401–422, 2023.
- [39] L. H. Nguyen and M. V. Klibanov. Carleman estimates and the contraction principle for an inverse source problem for nonlinear hyperbolic equations. *Inverse Problems*, 38:035009, 2022.
- [40] P. M. Nguyen, L. H. Nguyen, and H. T. Vu. Solving the inverse scattering problem via Carleman-based contraction mapping. *Computers and Mathematics with Applications*, 209:129–143, 2026.
- [41] J. R. Norris. Smoluchowski’s coagulation equation: uniqueness, nonuniqueness and a hydrodynamic limit for the stochastic coalescent. *The Annals of Applied Probability*, 9(1):78 – 109, 1999.
- [42] P. Olesen, J. Ferkinghoff-Borg, and J. Jensen, M. H. and Mathiesen. Diffusion, fragmentation, and coagulation processes: Analytical and numerical results. *Physical Review E*, 72(3):031103, 2005.
- [43] Benoit Perthame and Lenya Ryzhik. Exponential decay for the fragmentation or cell-division equation. *Journal of Differential Equations*, 210(1):155–177, 2005.
- [44] D. Ramkrishna. Drop-breakage in agitated liquid-liquid dispersions. *Chemical Engineering Science*, 29:987–992, 1974.
- [45] I.W. Stewart. On the coagulation-fragmentation equation. *Zeitschrift für angewandte Mathematik und Physik ZAMP*, 41(6):917–924, 1990.
- [46] H. V Tran and T.-S Van. Coagulation-fragmentation equations with multiplicative coagulation kernel and constant fragmentation kernel. *Communications on Pure and Applied Mathematics*, 75(6):1292–1331, 2022.
- [47] M.-B. Tran and B. Wang. Analysis of a numerical scheme for 3-wave kinetic equations. *arXiv preprint arXiv:2602.00264*, 2026.
- [48] D. D. Trong, L. H. Nguyen, and H. T. Vu. Determining initial conditions for nonlinear hyperbolic equations with time dimensional reduction and the Carleman contraction principle. *Inverse Problems*, 40:125021, 2024.
- [49] C. B. Van, T. T. Le, and L. H. Nguyen. The inverse initial data problem for anisotropic Navier–Stokes equations via Legendre time reduction method. *preprint arXiv:2507.16810*, 2025.
- [50] E. W. Montroll and R. Simha. Theory of depolymerization of long chain molecules. *The Journal of Chemical Physics*, 8:721–726, 09 1940.
- [51] H. Wright, R. Muralidhar, T. Tobin, and D. Ramkrishna. Inverse problems of aggregation processes. *Journal of statistical physics*, 61(3):843–863, 1990.
- [52] R. T. Zaks, S. A. Matveev, and V. P. Shutyaev. Fast numerical method for source function reconstruction in the coagulation–fragmentation equation. *Computational Mathematics and Mathematical Physics*, 65(7):1671–1690, 2025.
- [53] R.M. Ziff and E. D. McGrady. The kinetics of cluster fragmentation and depolymerisation. *J. Phys. A: Math. Gen*, 18:3027–3037, 1985.